Modification of Turbulent Helical/Non-Helical Flows with Small-Scale Energy Input

Yuji Suzuki* and Yasutaka Nagano**

**Department of Mechanical Engineering, the University of Tokyo,*

Hongo, Bunkyo-ku, Tokyo 113-8565, Japan

(Tel +81-3-5841-6411, Fax +81-3-5800-6999, e-mail ysuzuki@thtlab.t.u-tokyo.ac.jp)

***Department of Mechanical Engineering, Nagoya Institute of Technology,*

Gokiso-cho, Showa-ku, Nagoya 466-8555, Japan

PACS numbers: 47.27.Gs, 47.11.+j, 47.27.Ak, 47.27.Eq

ABSTRACT

Modification of helical/non-helical turbulence by adding small-scale turbulence is investigated with the aid of direct numerical simulations of isotropic turbulence. Detailed characteristics of the energy and helicity spectral transfer were examined. It is found that nonlocal energy cascade through isosceles triads toward the wave-number range of the energy input is markedly enhanced, thus the turbulent intensity is decreased faster than a flow field with no energy input. The optimum wave-number for turbulence reduction depends only on the characteristic wave-number of the energy-containing range, once the magnitude of the energy input is given. A model equation for isosceles triads derived from the EDQNM approximation indicates that the optimum wave-number increases with increasing energy ratio between the energy input and the parent turbulence. For helical turbulence, the sign of helicity is crucial for the helicity and energy transfer as well as the decay rate. When the helicity of small-scale energy input has the same sign as that of the parent turbulence, enhancement of the energy cascade is notedly deteriorated. The mechanism of suppressing interaction between the parent helical turbulence and the small-scale energy input is also explained with the aid of the EDQNM approximation.

I. INTRODUCTION

The nonlinear term of the Navier-Stokes equation is central to the dynamics of all turbulent flows and imposes well-known closure problems. In the energy equation in spectral space, the nonlinear term is expressed as vector triads among wave-numbers of wide range, and serves as interscale energy transfer. Since Kolmogorov, the notion of local energy cascade, i.e., turbulent kinetic energy is transferred from large scale to the neighboring smaller scale, remains an important element of the theory of turbulence. Domaradzki & Rogallo[1], Ohkitani & Kida[2], and Brasseur & Wei[3] obtained the details of energy transfer function in isotropic turbulence with the aid of direct numerical simulation (DNS) and showed that nonlocal triad interactions are predominant in local energy transfer. Zhou[4] claimed that contribution to the net flux in the inertial range is from relatively local interactions.

Recently, on the other hand, different energy transfer mechanisms found in various flows attracts much attention. Piomelli et al.[5] and Härtel et al.[6] evaluated subgrid scale models in their DNS databases and found that backward energy transfer, i.e., inverse cascade, is of great importance in transitional and turbulent wall flows, respectively. Nonlocal interaction is also believed to play an important role in turbulent flows, such as particle-laden[7,8] or bubble-laden[9] flows, astro- and geophysical flows[10], and turbulence with active control[11,12], where two energy feeding mechanisms with different scale coexist.

Turbulent flow passing through screens or grids is a classical problem and a huge amount of information has been accumulated[13-19]. In wind tunnel experiments, screens are mainly used to obtain uniform mean velocity distributions and/or reduce turbulence. There are three parameters for screens, i.e., mesh width, solidity, and the Reynolds number Re_d based on the wire diameter. When $Re_d<40$ (subcritical range), screens simply damp out fluctuations and hence turbulence is reduced[14]. On the other hand, when $Re_d>40$ (supercritical range), screens provide additional small-scale turbulence into the oncoming flow due to the vortex shedding and the shear layer instability. However, if the screen is sufficiently fine, turbulence can be suppressed downstream again. It is conjectured that the energy cascade from large scale (low wave-number) to smaller scale (higher wave-number) should be enhanced through the interaction of existing energy containing eddies with the small-scale turbulence fed by screens. However, the mesh size of screens used in wind tunnels could be much smaller than the turbulence length scale of the oncoming flow[17], so that the physical mechanism of reducing turbulence is not clearly shown and the optimum

controlling parameters, e.g., mesh size, for reducing turbulence still remain unknown.

Helicity is believed to be an important property of turbulent coherent structures[20,21]. Since high helicity density implies low energy cascade[22], it is often conjectured that coherent structures which contain helicity are long-lived. On the other hand, Rogers & Moin[23] examined helicity density in homogeneous shear flow and channel flows, and found no evidence of the correlation between low dissipation rate and high helicity density. However, Kasagi et al.[24] reported that near-wall streaky structures correspond well to high helicity density regions and anticipate that helicity plays an important role on the dynamics of turbulence. Therefore, if one can properly manipulate helicity density with external input, significant effect might be expected through selective manipulation of turbulent coherent structure.

The objectives of the present study are, i) to investigate turbulent modification by adding small-scale turbulence and clarify the detailed characteristics of spectral energy transfer, and ii) to examine the effect of helicity on nonlocal energy cascade when the additional turbulent energy is fed. To do this, we employ direct numerical simulations of decaying isotropic turbulence with/without helicity, and examine the effect of small-scale energy input systematically.

II. FUNDAMENTAL EQUATIONS

The energy equation for incompressible isotropic turbulence in the spectral space can be written as,

$$\left[\frac{\partial}{\partial t}+2\nu k^2\right]E(k)=T(k), \tag{1}$$

where $E(k)$, $T(k)$ and ν denote the energy spectrum, the energy transfer function, and the kinematic viscosity, respectively. The energy transfer function can be written as follows:

$$T(k)=\iint_{\Delta_k} T(k|p,q)\ dpdq, \tag{2}$$

where Δ_k refers to a domain in the p-q plane such that k, p, and q can be the sides of a triangle. The quantity $T(k|p,q)$ is the shell-averaged triad energy transfer function given by

$$T(k|p,q)=-\frac{1}{2}\sum \mathrm{Im}\left\{P_{ijm}(\boldsymbol{k})\hat{u}_i(\boldsymbol{k})\hat{u}_j(\boldsymbol{p})\hat{u}_m(\boldsymbol{q})\right\}\delta_{\boldsymbol{k}+\boldsymbol{p}+\boldsymbol{q}}, \tag{3}$$

with

$$P_{ijm}(\boldsymbol{k}) = k_m(\delta_{ij} - k_i k_j / k^2) + k_j(\delta_{im} - k_i k_m / k^2), \tag{4}$$

where $\hat{u}_i(\boldsymbol{k})$ and $\delta_{\boldsymbol{k}+\boldsymbol{p}+\boldsymbol{q}}$ respectively represent the Fourier coefficient of velocity and the Dirac δ function, and Σ denotes summation over spherical shells.

Helicity spectral density is defined as

$$H(k) = \sum \hat{u}_i(\boldsymbol{k}) \cdot \hat{\omega}_i(-\boldsymbol{k}), \tag{5}$$

where $\hat{\omega}_i(\boldsymbol{k})$ denotes the Fourier coefficient of vorticity. Unlike $E(k)$, $H(k)$ can be either positive or negative. It can also be shown that

$$|H(k)| \le 2kE(k). \tag{6}$$

The helicity density equation in the spectral space can be written in the form,

$$\left[\frac{\partial}{\partial t} + 2\nu k^2\right] H(k) = T_H(k), \tag{7}$$

where $T_H(k)$ denotes helicity transfer function,

$$T_H(k) = \sum \mathrm{Im}\left[-\frac{1}{2} P_{ijm}(\boldsymbol{k})\hat{\omega}_i(-\boldsymbol{k})\hat{u}_j(\boldsymbol{p})\hat{u}_m(\boldsymbol{q}) + k_j \hat{u}_i(\boldsymbol{k})\left\{\hat{u}_i(-\boldsymbol{p})\hat{\omega}_j(-\boldsymbol{q}) - \hat{u}_j(-\boldsymbol{p})\hat{\omega}_i(-\boldsymbol{q})\right\}\right]\delta_{\boldsymbol{k}-\boldsymbol{p}-\boldsymbol{q}}. \tag{8}$$

III. COMPUTATIONAL METHOD AND FLOW CONDITION

A. DNS

In order to examine the effect of small scale energy input on interscale energy transfer, we performed unique DNS of decaying isotropic turbulence with prescribed dominant scales. The computational procedure was almost the same as that of Rogallo[25]; Fourier-spectral methods were used for spatial representation and periodic boundary conditions were imposed in all three directions. Modified pressure was introduced to reduce computing time. Dealiasing was achieved by random phase shifting and spherical wave-space truncation. Number of computational mode was chosen as 128^3, thus the maximum wave-number given by $(2^{0.5}/3)N$ is 60.

The initial velocity fields were divergence-free and random, and had prescribed energy spectrum given as follows:

$$E(k) = \beta \cdot k_p{}^{-5} k^4 \exp\left\{-2\left(k / k_p\right)^2\right\}, \quad \beta = \frac{32}{3}\left(\frac{2}{\pi}\right)^{1/2} \qquad \text{for Case A,} \tag{9}$$

$$E(k) = \begin{cases} 0.25 & (k_m - 2 < k < k_m + 2) \\ 0 & (\text{otherwise}) \end{cases} \qquad \text{for Cases B and C.} \tag{10}$$

In both cases, the initial turbulent kinetic energy is set to unity.

For Cases A and B, helicity density was set to zero, while maximum helicity spectral density of positive sign, i.e., $2kE(k)$ ($\equiv H_{max}$) was given for Case C. In order to examine the effect of small-scale turbulence on interscale energy transfer, energy input having prescribed energy spectrum $E_c(k)$,

$$E_c(k) = \begin{cases} E_s & (k_c - 2 < k < k_c + 2) \\ 0 & (\text{otherwise}) \end{cases}, \tag{12}$$

and helicity spectral density $H_c(k)$,

$$H_c(k) = 0 \qquad \text{for Cases A and B,} \tag{13}$$

$$H_c(k) = 0,\ 2kE(k),\ -2kE(k) \qquad \text{for Case C,} \tag{14}$$

was added into the initial velocity field. In the present DNSs, E_s was chosen as 0.25, thus the turbulent kinetic energy in the small scale is also unity.

The computational parameters are summarized in Table. 1. The kinematic viscosity and the time step was respectively chosen as 6.3479×10^{-3} and 1.25×10^{-3}, respectively. The initial Taylor microscale Reynolds numbers Re_λ without the small-scale energy input were 81, 93 and 93 for Cases A, B, and C, respectively. For Case C, the initial helical field was generated with the same procedure as Polifke & Shtilman[26].

B. EDQNM

When examining the effect of small-scale energy input for various parameters systematically, numerical simulation with the eddy-damped quasi-normal Markovian (EDQNM) model[27,28] was adapted in order to reduce computational cost. The EDQNM model has been shown to be consistent with DNS results in

the inertial subrange[1,2] and the dissipation range[29]. Suzuki & Nagano[30] show that the EDQNM model can also predict both forward and backward energy cascade reasonably well for decaying isotropic turbulence.

By using the EDQNM approximation (André & Lesieur[22]), one can rewrite Eq. (3) as

$$T(k|p,q) = \vartheta_{kpq}\frac{k}{pq}b(k,p,q)E(q)\left\{k^2E(p) - p^2E(k)\right\} - \vartheta_{kpq}\frac{k}{p^3q}c(k,p,q)H(q)\left\{k^2H(p) - p^2H(k)\right\}, \tag{15}$$

where usual notations are used for ϑ_{kpq}, $b(k,p,q)$ and $c(k,p,q)$, i.e.,

$$\vartheta_{kpq} = \frac{1 - e^{-\left\{\mu_{kpq} + \nu(k^2+p^2+q^2)\right\}t}}{\mu_{kpq} + \nu(k^2+p^2+q^2)}, \tag{16}$$

$$b(k,p,q) = (xy + z^3)p/k, \tag{17}$$

$$c(k,p,q) = z(x + yz)p^2/(kq). \tag{18}$$

The quantities x, y, and z are the cosines of angles facing sides k, p, and q of a triangle, respectively. In Eq. (16), the second term of the numerator is often neglected when time t is large. However, we retain this term in order to calculate decaying turbulence. The following expression was employed for the eddy-damping rate μ_{kpq},

$$\mu_{kpq} = \mu_k + \mu_p + \mu_q,\ \mu_k = \lambda\left\{\int_0^k k'^2 E(k')dk'\right\}^{1/2}, \tag{19}$$

where the adjustable constant λ was chosen as 0.37 to keep the Kolmogorov constant at 1.8 as suggested by Kida et al.[29] For non-helical flows, Eq. (15) reduces to

$$T(k|p,q) = \vartheta_{kpq}\frac{k}{pq}b(k,p,q)E(q)\left\{k^2E(p) - p^2E(k)\right\}. \tag{20}$$

IV. MODIFICATION OF NON-HELICAL TURBULENCE

A. Temporal evolution of turbulent statistics

Figures 1 (a) and (b) respectively show time evolution of energy spectra in Case A. While the initial spectrum with the small-scale energy input has two energy peaks and a trough in between, the peak around k_c is smeared out at t>0.5 (Fig. 1b). The turbulent kinetic energy at the largest scale (k=1) for k_c=11.5 is much less than that for the unmanipulated case at t>0.5. This fact indicates that the small-scale energy input prevents the large-scale energy from transferring backward during the initial period of decay. Spectra exhibit a similar shape at t>1.0 for both cases and decay uniformly at the later time. Most features mentioned above are also observed in Case B as shown in Figs. 1 (c) and (d), whereas initial spectra are quite different.

Time traces of the turbulent kinetic energy K with various wave-numbers k_c for the small-scale energy input are shown in Fig. 2. Whereas the initial turbulent energy has doubled in manipulated cases, K becomes smaller than the unmanipulated case when t > 0.4 - 0.9. The decay rate between t=1.7 and 3.0 is respectively $t^{-1.1}$ and $t^{-1.2}$ for Cases A and B without the small-scale energy input, but it is increased to $t^{-1.4}$ with the small-scale energy input of k_c=11.5 for both cases. Figure 3 shows time traces of the ratio K/K_0 for various k_c, where K_0 is the turbulent kinetic energy for the unmanipulated case. It is evident that turbulent reduction can actually be obtained by adding small-scale turbulence, and 20 - 30% reduction is obtained at around t=2.0. There exists an optimum value of k_c ($k_{c,opt}$=11.5 for this case), as we discuss later in Sec. IVc. The maximum turbulent reduction rate obtained for Case B is somewhat larger than that for Case A. It is conjectured that the interaction between the two energy bands is more active in Case B than in Case A, since the turbulence energy at low wave-numbers is concentrated in a narrow wave-number range. In the next section, we focus on Case A for further analysis.

B. Characteristics of interscale energy transfer

Figure 4 (a) shows the energy transfer function $T(k)$ for Case A at t=0.1. For the unmanipulated case, turbulent kinetic energy is transferred forward from the wave-number rage of 2<k<8, where $T(k)$ is negative, to the wave-number range of 8<k<15, where $T(k)$ is positive. With the small-scale energy input of k_c=11.5,

the negative peak at around k=5 becomes much larger. Thus, the energy cascade from the energy-containing scale is markedly enhanced. A large negative peak in $T(k)$ at $10<k<13$ corresponds to the energy loss from the small-scale energy input, which is transferred both forward and backward. At t=0.5, the negative peak at around k=12 disappears and the energy loss around k=5 becomes the same level for both cases (Fig. 4b). On the other hand, the energy gain is concentrated in the higher wave-number range for the manipulated case with k_c=11.5. The distributions become similar for both cases at t=1.0, while the magnitude for k_c=11.5 is smaller than the unmanipulated case due to the lower turbulent energy at this time step (Fig. 4c). Therefore, the direct effect of the small-scale energy input is confined only in the initial period of decay, when the forward energy transfer from the energy containing range is enhanced. On the other hand, the decay rate is increased even after this period, since more turbulent energy is concentrated in the higher wave-number range, where the dissipation is predominant.

Figure 5 shows contours of the triad transfer function $T(k|p,q)$ at k=5, where the energy loss is maximum as shown in Fig. 4 (a). Three solid lines represents the boundary of the triangular condition extended owing to finite shell width of 0.5, where three wave-numbers k, p, and q can form a triangle. For the unmanipulated case, strong positive triad interactions are observed at around p~q~3, which corresponds to gain with forward local energy transfer to k=5. In the wave-number region of $5<p<10$ and $5<q<10$, $T(k|p,q)$ is negative, so that turbulent energy is redistributed to somewhat wide wave-number range. In this range, the scale disparity parameter[4] defined as

$$s(k,p,q)=\frac{\max(k,p,q)}{\min(k,p,q)} \tag{21}$$

is less than 2, thus contributions of nonlocal interaction is minor in this case. It is also noted that there exist regions of weak nonlocal interaction at around (p, q)~(2, 6) and (6, 2), which corresponds to local energy transfer as reported in the previous results[2-4].

When the small-scale energy input at k_c=11.5 is applied, the distributions of $T(k|p,q)$ at $p, q < 10$ is not strongly affected. However, $T(k|p,q)$ at $p, q > 10$ changes significantly; $T(k|p,q)$ becomes negative in the wave-number range of $10<p, q<15$ (s=2~3). This fact indicates that turbulent energy in the energy containing range around k_p is nonlocally transferred toward k_c, whereas the wave-number range around

k_c contains large turbulent energy.

At k=9, where the energy gain is maximum, $T(k|p,q)$ is positive at $p, q < 10$ for the unmanipulated case as shown in Fig. 6 (a). On the other hand, backward energy transfer from the wave-number range of the small-scale energy input is evident for k_c=11.5 (Fig. 6b). Note that contributions from nonlocal interactions having peaks at (p, q)~(4, 11) and (11, 4) are dominant in the backward transfer if compared with the local interactions p~q~11.

Figures 7 (a) and (b) respectively show $T(k|p,q)$ for the manipulated case at k=12 and k=16. At k=12 where the energy loss is maximum, $T(k|p,q)$ has large negative peaks at (p, q)~(5, 14) and (14, 5). Since the magnitude of $T(k|14,12)$ and $T(k|12,14)$ at k=5 is small as shown in Fig. 5 (b), the energy loss at k=12 is mostly transferred to the higher wave-number range (k~14) through nonlocal interactions (s=2~3). It is also noted that there exists gain at around (p, q)~(5, 10) and (10, 5), which corresponds to nonlocal transfer from the energy containing range (k~5) as mentioned above. At k=16, $T(k|p,q)$ is positive at $p, q < 16$, while negative at around (p, q)~(5, 18) and (18, 5). Therefore, the energy is gained through various local and nonlocal interactions, while contribution of nonlocal interactions is dominant in the loss of energy toward smaller scales.

C. Optimum scale of energy input for reducing turbulence

In order to determine the optimum wave-number $k_{c,opt}$ for various initial energy spectrum systematically, numerical simulations were made based on the EDQNM approximations described in Sec. IIIb. The characteristic wave-numbers k_p and k_m were changed up to 14, and Re_λ of the initial unmanipulated field was changed between 58 and 197. The energy level E_s in the wave-number range of the small-scale energy input is chosen as 0.25, 1.25, 2.5, 5 and 10 (up to 40 times larger than that for DNS), while the highest wave-number for the computation was chosen as 230.

Figure 8 shows the comparison of time traces of turbulent kinetic energy and its dissipation rate between DNS and EDQNM. In the unmanipulated case, the result of EDQNM is in excellent agreement with that of DNS. On the other hand, with the small-scale energy input, EDQNM somewhat overestimates the dissipation rate in the wave-number range of the energy input in the initial period of decay. Thus, the energy cascade due to the nonlocal interaction at the later period is slightly underestimated, which results

in larger turbulent kinetic energy when compared with that of DNS. However, the optimum scale ratio is proved to be unchanged between EDQNM and DNS, so that the present EDQNM calculation can be used for identifying optimum scale of energy input to reduce turbulence.

In Figure 9, $k_{c,opt}$ for E_s=1.25 is plotted against k_p or k_m. All data for $k_{c,opt}$ have a strong correlation with k_p or k_m, and the ratio between the two wave-numbers is about 2.3. This fact indicates that the optimum scale of the small-scale energy input is closely related with the scale of the energy-containing eddies. The maximum turbulence reduction rate with $k_{c,opt}$ is larger for Case B than for Case A, and between 20-30% depending on k_p or k_m (Fig. 10). Note that EDQNM computations give somewhat lower reduction rate compared with the DNS data, but the general trend can be reproduced with the present simulations.

Since isosceles triad interaction has large contribution to the nonlocal energy transfer as shown in Fig. 5 (b), we examined the optimum scale for isosceles triads with the aid of the EDQNM approximation. In the present analysis, we employ a simple form for θ_{kpq}[27] given by

$$\vartheta_{kpq} = \left\{ \mu_{kpq} + \nu(k^2 + p^2 + q^2) \right\}^{-1}, \tag{22}$$

where

$$\mu_{kpq} = \mu_k + \mu_p + \mu_q, \ \mu_k = \lambda' \left(k^3 E(k) \right)^{1/2}, \tag{23}$$

instead of Eqs. (20) and (19), respectively. Assuming p=q (>k), and neglecting the molecular viscous term in Eq. (22), since the Re number $(E(k)/k)^{1/2} / \nu$ >>1, then the nondimensionalized triad energy transfer function defined by $T^*(r, E^*) = T(k,p,q) / \left\{ E(k)^{3/2} / k^{1/2} \right\}$ can be written as follows:

$$T^*(r, E^*) = \frac{1}{8\lambda'} \cdot \frac{E^{*3/2} \cdot r^{-3/2} (4 - r^{-2})(r^{-2} - E^{*-1})}{E^{*-1/2} \cdot r^{-3/2} + 2}, \tag{24}$$

where r=p/k and E^*=$E(p)/E(k)$ are respectively the wave-number ratio and the energy ratio. The range of the parameter r is r>0.5 due to the triangle condition. We further assume the wave-numbers k and p are respectively in the energy-containing range and the range of the small-scale energy input, and examine

the energy transfer from the energy-containing range by using Eq. (24).

Figure 11 shows distributions of T^* for various E^*. The quantity T^* becomes zero at $1/r=0$, $E^{*-1/2}$, and 2. Therefore, at $0<1/r<E^{*-1/2}$ where T^* is negative, the turbulent energy at k is transferred to the higher wave-number p; the nonlocal transfer with the isosceles triads can enhance the forward cascade in this case. The condition $1/r< E^{*-1/2}$ can also be derived from the non-local expansion of the transfer function[28] except small discrepancy in the numerical coefficient (see Appendix).

When $r=r_{min}$ is chosen such that T^* becomes local minimum (i.e., $dT^*/dr=0$), maximum energy extraction from the wave-number k, and hence maximum turbulent reduction is expected. Figure 12 shows the wave-number ratio r_{min} versus E^*. Roots of the equation $dT^*/dr=0$ were calculated numerically by using the Newton method. The quantity r_{min} is increased with E^*, and in good agreement with the correlation,

$$r_{\min} = 0.17 + 1.5E^{*0.5}. \tag{25}$$

Therefore, with increasing energy ratio of the small-scale energy input to that of the parent flow, its scale ratio should also be increased to obtain optimum turbulent reduction. The optimum wave-number ratios obtained with the present DNS and EDQNM simulations are also plotted in Fig. 12. They exhibit similar trend, however, the exponent is much smaller than that of Eq. (25), and is about 0.2. The empirical correlation for the EDQNM results can be written as,

$$r_{\min} = 0.2 + 1.6E^{*0.2} \tag{26}$$

In the present analysis, the optimum scale for the maximum energy transfer is estimated by using the initial value of E^*. However, as turbulence decays, the energy peak of the small-scale energy input is quickly smeared out due to the viscous dissipation and/or the interscale energy transfer as shown in Figs 1 (b) and (d), i.e., E^* is rapidly decreased in time. Therefore, the optimum scale for turbulence reduction should also be decreased gradually. This could be the reason why the present simple analysis overestimates the optimal wave-number ratio. It is also noted that the viscous term neglected when Eq. (24) was derived has little contribution to T^* and hence r_{min}.

Although Eqs (25) and (26) derived in the spectral space could not be readily translated into the counterpart in the physical space, they should provide a clue to evaluate the effect of nonlocal energy cascade. For instance, the order of the optimum mesh size of screens in a wind tunnel can be estimated by using Eq. (26) as follows: when we assume that all energy loss at the screen is converted into the turbulent energy, and that the pressure coefficient of the screen is unity, the turbulent kinetic energy generated is as large as the free stream kinetic energy. Then, when the free stream turbulent intensity of the oncoming flow is 0.1%, the energy ratio E^* is as large as 10^6, and the optimum scale ratio r predicted by Eq. (26) is 26. Therefore, the optimum values for the mesh width or the wire diameter could be one or two order of magnitude smaller than the turbulent length scale of the oncoming flow. Although the present estimates is rather rough, but the reason why fine screens are effective in reducing turbulence could be qualitatively explained.

V. MODIFICATION OF HELICAL TURBULENCE

Figure 13 shows time trace of turbulent kinetic energy K and its dissipation rate ε in Case C for unmanipulated case. For helical case ($H(k)=H_{max}$), the growth rate of ε is markedly decreased, and the buildup of enstropy is suppressed. Thus, the decay of K is much slower than that for the non-helical case as Polifke & Shtilman[26] reported. In this section, the wave-number of the small-scale energy input k_c was kept constant as 11.5, which is most effective in non-helical cases.

Figure 14 shows temporal evolution of helicity spectral density $H(k)$. In the unmanipulated case, the helicity cascade is fairly small, and $H(k)$ decays slowly due to the viscous dissipation. On the other hand, when the small-scale energy input is applied, the evolution of $H(k)$ strongly depends on the sign of $H_c(k)$; for $H_c(k)=-H_{max}$, $H(k)$ at $2<k<6$ decays more rapidly than that for the unmanipulated case, while the rate of decay for $H_c(k)=H_{max}$ is not much changed at $t<0.2$.

Time traces of K and ε are shown in Fig. 15. In helical cases, the decay of K is markedly accelerated when the small-scale energy input is applied, while the turbulence reduction rate depends strongly on the sign of $H_c(k)$ again; K/K_0 at $t=3$ is respectively 53%, 64%, and 44% for $H_c(k)=0$, $-H_{max}$, and H_{max}. The dissipation rate ε for $H_c(k)=H_{max}$ is smaller than the other cases at $t<0.5$.

These facts along with distributions of the energy and the helicity transfer function shown in Figs 16

and 17 indicates that when the helicity of the small-scale energy input has the opposite sign to that of the energy-containing range, both helicity and energy cascade are enhanced through the interaction with the small-scale energy input. Tur & Levich[31] found in their DNS that this is also the case for decaying isotropic turbulence with zero initial helicity. On the other hand, when the signs are the same, the helicity cascade is fairly slow especially at the low wave-number range, so that the energy cascade is suppressed by the action of helicity if compared with the non-helical case ($H_C(k)$=0). Note that the effect of the small-scale energy input is significant during the initial period of decay as non-helical cases, and the distributions of $T(k)$ and $T_H(k)$ become similar at t>1.0 as shown in Fig. 16 (b). It is also noted that when $H_C(k)=H_{max}$, the gain in helicity density at around k~8 is much larger than the loss at k<6. Therefore, the backward helicity cascade from the wave-number range of the energy input should occur (Fig. 17c).

Figure 18 (a) shows the triad transfer function $T(k|p,q)$ at k=5 for $H_C(k)=-H_{max}$. Substantial nonlocal transfer with the isosceles triad interaction (p~q~11), which is also observed in the non-helical case (Fig. 5b) is evident, while local energy cascade at p, q<10 is suppressed by the action of helicity. On the other hand, when $H_C(k)=H_{max}$, distributions of $T(k|p,q)$ change dramatically as shown in Fig. 18 (b). The peak corresponding to the isosceles triad interactions levels off, and splits into two plateaus near the boundary. Moreover, there exist strong positive triad interactions at around (p, q)~(15,12) and (12,15), which correspond to the backward energy transfer to k=5.

The suppression of the isosceles triad interaction mentioned above can also be explained by using the EDQNM approximation. When we assume the wave-number k is in the energy-containing range, while p and q are in the wave-number range of the energy input (p=q), and follows the same procedure as in Sec. IIIc, then Eq. (15) can be written as

$$T^*(r,E^*,H^*,H_{Rk}) = \frac{1}{8\lambda'}\cdot\frac{E^{*3/2}\cdot r^{-3/2}(4-r^{-2})}{E^{*-1/2}\cdot r^{-3/2}+2}\left\{\left(r^{-2}-E^{*-1}\right)-4H_{Rk}^2H^{*2}\frac{1}{r}\left(\frac{1}{r}-\frac{1}{H^*E^*}\right)\right\}, \quad (27)$$

where H_{Rk} and H_{Rp} are respectively the relative helicity ($=H(k)/(2kE(k))$) at the wave-number k and p, while H^* is their ratio ($=H_{Rp}/H_{Rk}$). When the signs of $H(k)$ and $H(p)$ are the same, then H^*>0, and vice versa. For the isosceles triad interactions we consider, the first term in the bracket of Eq. (27), (r^{-2}-E^{*-1}) is negative, which corresponds to the forward energy cascade. When H^*<0, the second term is always

negative, which aids the first term. On the other hand, when $H^*>r/E^*$, the second term becomes positive, which would cancel out with the first term, or even contribute to the backward energy transfer. Since we consider the period of r as $0<1/r<E^{*-1/2}$, the necessary condition of suppressing isosceles triads with helicity should be

$$H^* > E^{*-1/2}. \tag{28}$$

Figure 19 shows the distributions of T^* for $H_{Rk}=1$ and $H^*=E^{*-1/2}$. If compared with Fig. 11, it indicates that the energy transfer can be actually reduced when $H^*>0$. However, the effect should be decreased with increasing E^*, since the magnitude of H^* and hence the relative helicity H_{Rp} are also decreased.

VI. CONCLUSIONS

Modification of helical/non-helical turbulence by adding small-scale turbulence was studied by using direct numerical simulations of decaying isotropic turbulence. The following conclusions are established:

1) Turbulent intensity can be decreased by adding turbulence kinetic energy into smaller scales. Relevant nonlocal energy cascade toward the wave-number range of the small-scale energy input is remarkably enhanced through isosceles triad interactions during the initial period of decay.
2) The optimum wave-number for turbulence reduction depends only on the characteristic wave-number of the energy-containing range, once the magnitude of the energy input is given. A model equation for isosceles triads derived from the EDQNM approximation indicates that the optimum wave-number is increased with increasing energy ratio. An empirical formula for the optimum wave-number is also obtained by using the EDQNM simulations with various initial conditions.
3) For helical turbulence, the sign of helicity is crucial to the helicity and energy transfer as well as the decay rate. When helicity of the small-scale energy input has the same sign as that of the parent turbulence, enhancement of the nonlocal energy cascade becomes markedly deteriorated. The necessary condition of relative helicity for suppressing isosceles triads is given as a function of the energy ratio based on the EDQNM approximation.

The present study is focused on the physics of interscale energy transfer in isotropic turbulence, and dynamics of nonlocal interaction is examined in the spectral space. Thus, it is not straightforward to interpret the present result into turbulence phenomena in the physical space. However, the well-known observations that fine screens are effective in reducing large-scale turbulence in wind tunnels are qualitatively explained with the model equation of the scale ratio for the maximum forward cascade. Therefore, the mechanism of nonlocal interaction presently obtained can be a clue to investigate turbulent flow field where nonlocal transfer between two dominant scales is important.

ACKNOWLEDGMENTS

The authors are grateful to Mr. S. Yamada for his cooperation in the DNS code. The financial support through the Grant-in-Aid for Scientific Research on Priority Areas from the Ministry of Education, Science and Culture of Japan (No. 05240103) is also acknowledged.

APPENDIX: Nessesary condition for the forward cascade enhancement derived from a nonlocal expansion of the transfer function

Lesieur[28] has derived the transfer function with nonlocal interactions $k << p \sim q$ from a nonlocal expansion of Eq. (20), which gives the dominant terms as follows:

$$T_{NL}(k) = -\frac{2}{15}k^2 E(k)\int_{k_i}^{\infty}\theta_{kpp}\left\{E(p) + p\frac{\partial E}{\partial p}\right\}dp + \frac{14}{15}k^4\int_{k_i}^{\infty}\theta_{kpp}\frac{E(p)^2}{p^2}dp. \qquad \text{(A-1)}$$

In Eq. (A-1), the net transfer is determined by a balance between two different mechanism. The first term represents spectral eddy-viscosity of the form $-2\nu_t k^2 E(k)$, which damps large scale fluctuations. On the other hand, the second term corresponds to the backward energy cascade due to the beating mode. In the present study, the energy input in the high wave-number range can enhance the foward cascade if $T_{NL}(k)<0$.

When we assume $5E(p) >> p\frac{\partial E}{\partial p}$ for simplicity, and use Eq. (22) for θ_{kpq}, then the nessesary condition

for $T_{NL}(k)<0$ becomes

$$1/r < \left(\frac{7}{5}\right)^{1/2} E^{*-1/2}, \qquad \text{(A-2)}$$

which is equivalent with the condition $T(k|p,q)>0$ except the numerical coefficient of $(7/5)^{0.5}$.

REFERENCES

[1]J. A. Domaradzki, and R. S. Rogallo, "Local energy transfer and nonlocal interactions in homogeneous isotropic turbulence," Phys. Fluids A **2**, 413 (1990).

[2]K. Ohkitani, and S. Kida, "Triad interactions in a forced turbulence," Phys. Fluids A **4**, 794 (1992).

[3]J. G. Brasseur, and C.-H. Wei, "Interscale dynamics and local isotropy in high Reynolds number turbulence within triadic interactions," Phys. Fluids **6**, 842 (1994).

[4]Y. Zhou, "Interacting scales and energy transfer in isotropic turbulence," Phys. Fluids A **5**, 2511 (1993).

[5]U. Piomelli, W. H. Cabot, P. Moin, and S. Lee, "Subgrid-scale backscatter in turbulent and transitional flow," Phys. Fluids *A* **3**, 1766 (1991).

[6]C. Härtel, L. Kleiser, F. Unger, and R. Friedrich, "Subgrid-scale energy transfer in the near-wall region of turbulent flow," Phys. Fluids **6**, 3130 (1994).

[7]S. Elghobashi, and G. C. Truesdell, "On the two-way interaction between homogeneous turbulence and dispersed solid particles," Phys. Fluids A **5**, 1790 (1993).

[8]S. Schreck, and S. Kleis, "Modification of grid-generated turbulence by solid particles," J. Fluid Mech. **249**, 665 (1993).

[9]A. Esmaeeli, and G. Tryggvason, "An inverse energy cascade in two-dimensional low Reynolds number bubbly flow," J. Fluid Mech. **314** 315 (1996).

[10]A. Pouquet, U. Frisch, and J. P. Chollet, "Turbulence with a spectral gap," Phys. Fluids **26** 877 (1983).

[11]S. P. Wilkinson, "Interactive wall turbulence control," in *Prog. Astronautics and Aeronautics: Viscous Drag Reduction in Boundary Layers*, D. M. Bushnell, and J. N. Hefner, eds., (AIAA, 1990), Vol. **123**, pp. 479-509.

[12]P. Moin, and T. Bewley, "Feedback control of turbulence," Appl. Mech. Rev., **47**, S3 (1994).

[13]H. L. Dryden, and G. B. Schubauer, "The use of damping screens for the reduction of wind-tunnel turbulence," J. Aero. Sci. **14**, 221 (1947).

[14]G. I. Taylor, and G. K. Batchelor, "The effect of wire gauze on small disturbances in a uniform stream," Q. J. Mech. Appl. Maths **2**, 1 (1949).

[15]W. D. Baines, and E. G. Peterson, "An investigation of flow through screens," Trans. ASME **73**, 467 (1951).

[16]P. Bradshaw, "The effect of wind-tunnel screens on nominally two-dimensional boundary layers," J. Fluid Mech. **22**, 679 (1965).

[17]E. M. Laws, and J. L. Livesey, "Flow through screens," Ann. Rev. Fluid Mech. **10**, 247 (1978).

[18]J. Tan-Atichat, H. M. Nagib, and R. I. Loehrke, "Interaction of free-stream turbulence with screens and grids: a balance between turbulence scales," J. Fluid Mech. **114**, 501 (1982).

[19]J. Groth, and A. V. Johansson, "Turbulence reduction by screens," J. Fluid Mech., **197** 139 (1988).

[20]J. C. R. Hunt, and F. Hussain, "A note on velocity, vorticity and helicity of inviscid fluid elements," J. Fluid Mech. **229**, 569 (1991).

[21]H. K. Moffatt, and A. Tsinober, "Helicity in laminar and turbulent flow," Annu. Rev. Fluid Mech. **24**, 281 (1992).

[22]J. C. André, and M. Lesieur, "Influence of helicity on the evolution of isotropic turbulence at high Reynolds number," J. Fluid Mech. **81**, 187 (1977).

[23]M. M. Rogers, and P. Moin, "Helicity fluctuations in incompressible turbulent flows," Phys. Fluids **30**, 2662 (1987).

[24]N. Kasagi, Y. Sumitani, Y. Suzuki, and O. Iida, "Kinematics of the quasi-coherent vortical structure in near-wall turbulence," Int. J. Heat & Fluid Flow **16**, 2 (1995).

[25]R. S. Rogallo, "Numerical experiments in homogeneous turbulence," NASA TM-81315 (1981)

[26]W. Polifke, and L. Shtilman, "The dynamics of helical decaying turbulence," Phys. Fluids *A* **1**, 2025 (1989).

[27]S. A. Orzag, "Analytical theories of turbulence," J. Fluid Mech. **41**, 363 (1970).

[28]M. Lesieur, *Turbulent in Fluids, 3rd ed.*, (Martinus Nijihoff, Dordrecht, The Netherlands, 1997).

[29]S. Kida, R. H. Kraichnan, R. Rogallo, F. Waleffe, and Y. Zhou, "Triad interactions in the dissipation

range," in *Proc. 1992 Summer Program*, (CTR, Stanford University, 1992), pp. 83-99.

[30]Y. Suzuki, and Y. Nagano, "On the spectral transfer function for backward energy cascade in turbulence," in *Proc. 10th Turbulent Shear Flows*, F. Durst et al., eds., (Penn. State, 1995), pp. 17.19-17.24.

[31]A. V. Tur, and E. Levich, "The Origin of Organized Motion in Turbulence," Fluid Dyn. Res. **10**, 75 (1992).

Table 1: Computational parameters for DNS.

	Grid Points N^3	E_s	k_p, k_m	k_c	$H(k)$	$H_c(k)$
Case A	128^3	0.25	k_p=4.76	9.5 - 19.5	0	0
Case B			k_m=4.5		0	0
Case C				11.5	$2kE(k)$	0, $2kE(k)$, $-2kE(k)$

Figure 1: Temporal evolution of energy spectra. (a) Case A (k_p=4.76, Unmanipulated case), (b) Case A (k_p=4.76, k_c=11.5), (c) Case B (k_m=4.5, Unmanipulated case), (b) Case B (k_m=4.5, k_c=11.5).

Figure 2: Time trace of turbulent kinetic energy. (a) Case A (k_p=4.76), (b) Case B (k_m=4.5).

Figure 3: Time trace of turbulent kinetic energy normalized with that for the unmanipulated case. (a) Case A (k_p=4.76), (b) Case B (k_m=4.5).

Figure 4: Temporal evolution of energy transfer function for Case A (k_p=4.76, k_c=11.5). (a)t=0.1, (b)t=0.5, (c)t=1.0.

Figure 5: Triad transfer function for Case A (k_p=4.76, k=5) at t=0.1. (a)Unmanipulated case, (b) k_c=11.5.

Figure 6: Triad transfer function for Case A (k_p=4.76, k=9) at t=0.1. (a)Unmanipulated case, (b) k_c=11.5.

Figure 7: Triad transfer function for Case A (k_p=4.76, k_c=11.5) at t=0.1. (a)k=12, (b)k=16.

Figure 8: Time trace of turbulent kinetic energy and dissipation rate for Case A (k_p=4.76) for comparison of EDQNM and DNS. (a) Unmanipulated case, (b)k_c=11.5.

Figure 9: Optimum wave-number $k_{c,opt}$ versus characteristic wave-numbers for Cases A and B.

Figure 10: Maximum energy reduction rate $(K/K_0)_{\min}$ versus characteristic wave-numbers for Cases A and B.

Figure 11: Distribution of nondimensionalized triad energy transfer function $T^*=T^*(r,E^*)$ of isosceles interactions.

FIgure 12:Optimum wave-number of control input versus turbulent energy ratio.

Figure 13: Time trace of turbulent energy K and its dissipation rate ε for Case C without control input. (a) K , (b) ε.

Figure 14: Temporal evolution of helicity spectral density for Case C. (a) Unmanipulated case, (b) H_c=-H_{max}, (c) H_c=H_{max}.

Figure 15: Time trace of turbulent kinetic energy K and its dissipation rate ε for Case C. (a) K, (b) ε.

Figure 16: Temporal evolution of energy transfer function for Case C. (a)t=0.1, (b)t=1.0

Figure 17: Temporal evolution of helicity transfer function for Case C. (a)H_c=0, (b)H_c=-H_{max}, (c)Hc=H_{max}.

Figure 18: Triad transfer function for Case C at t=0.1. (a)H_c=-H_{max}, (b)H_c=H_{max}.

Figure 19: Distribution of nondimensionalized triad energy transfer function $T^*=T^*(r,E^*,H^*,H_{Rk})$ for helical case (H_{Rk}=1).

(a)

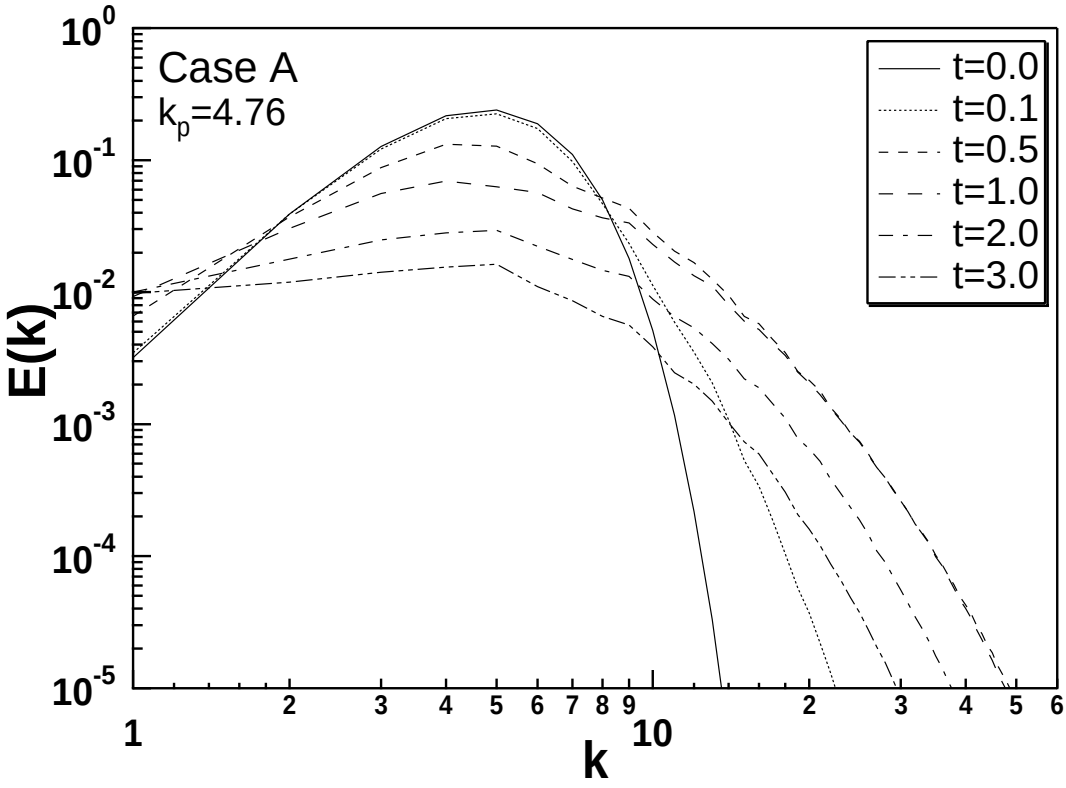

(b)

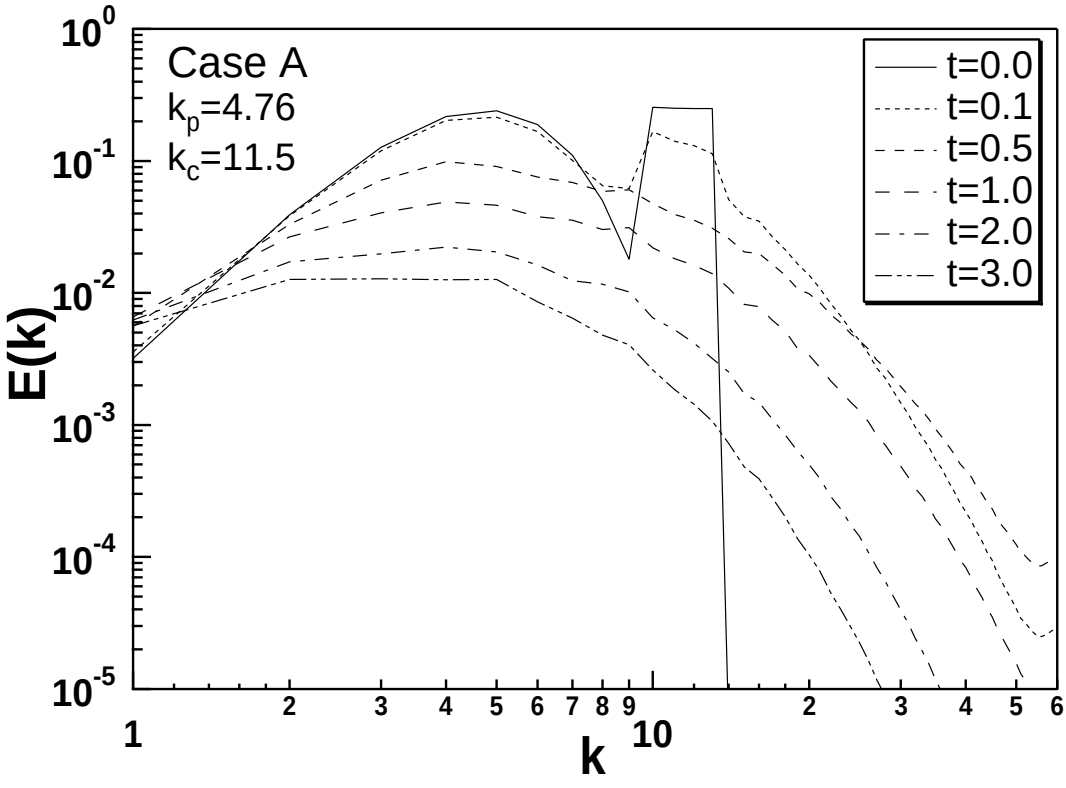

Figure 1: Temporal evolution of energy spectra. (a) Case A (k_p=4.76, Unmanipulated case), (b) Case A (k_p=4.76, k_c=11.5).

(c)

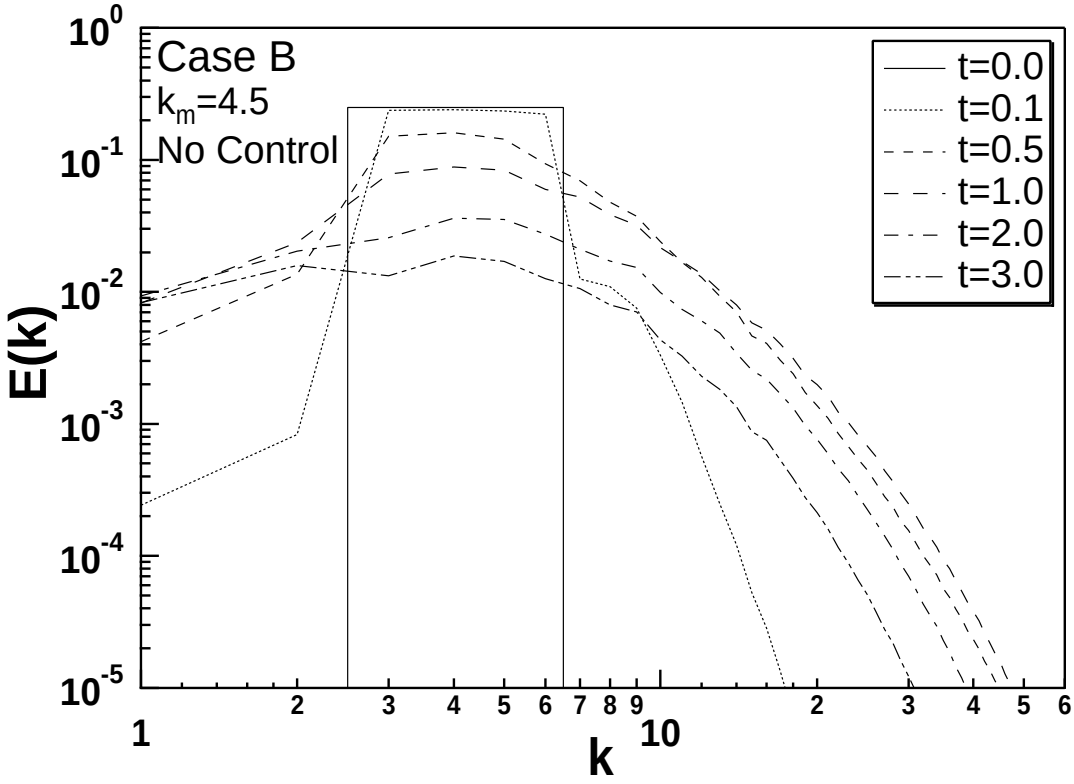

(d)

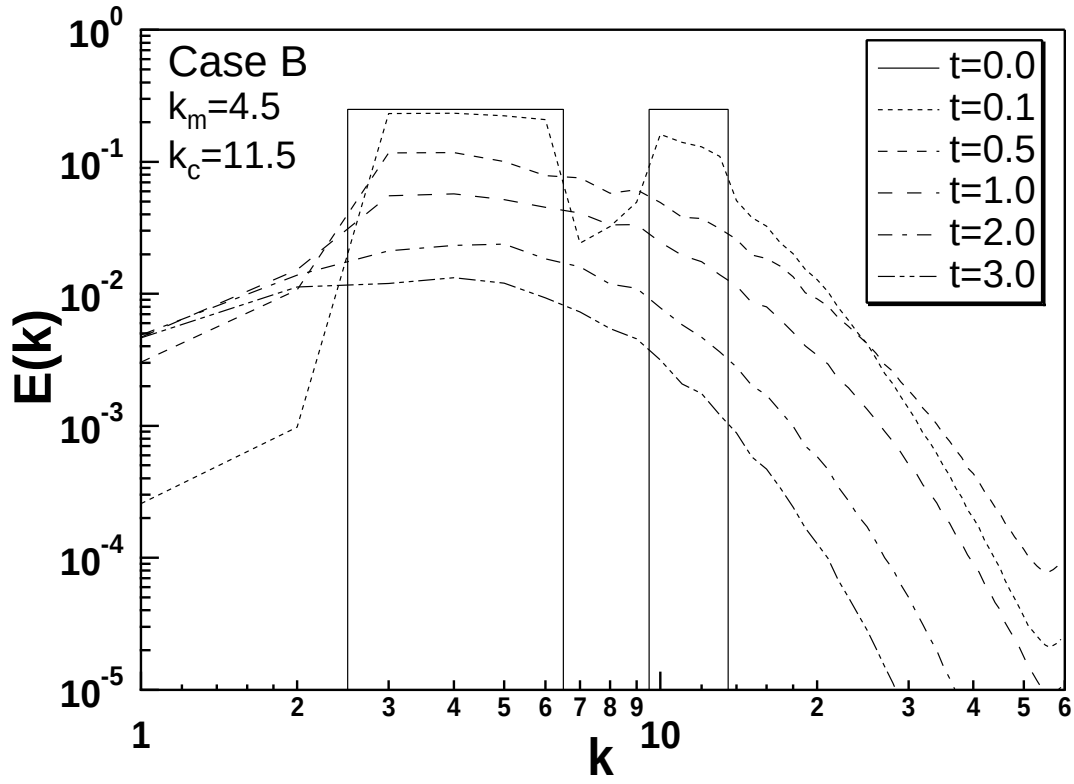

Figure 1: (c) Case B (k_m=4.5, Unmanipulated case), (b) Case B (k_m=4.5, k_c=11.5).

(a)

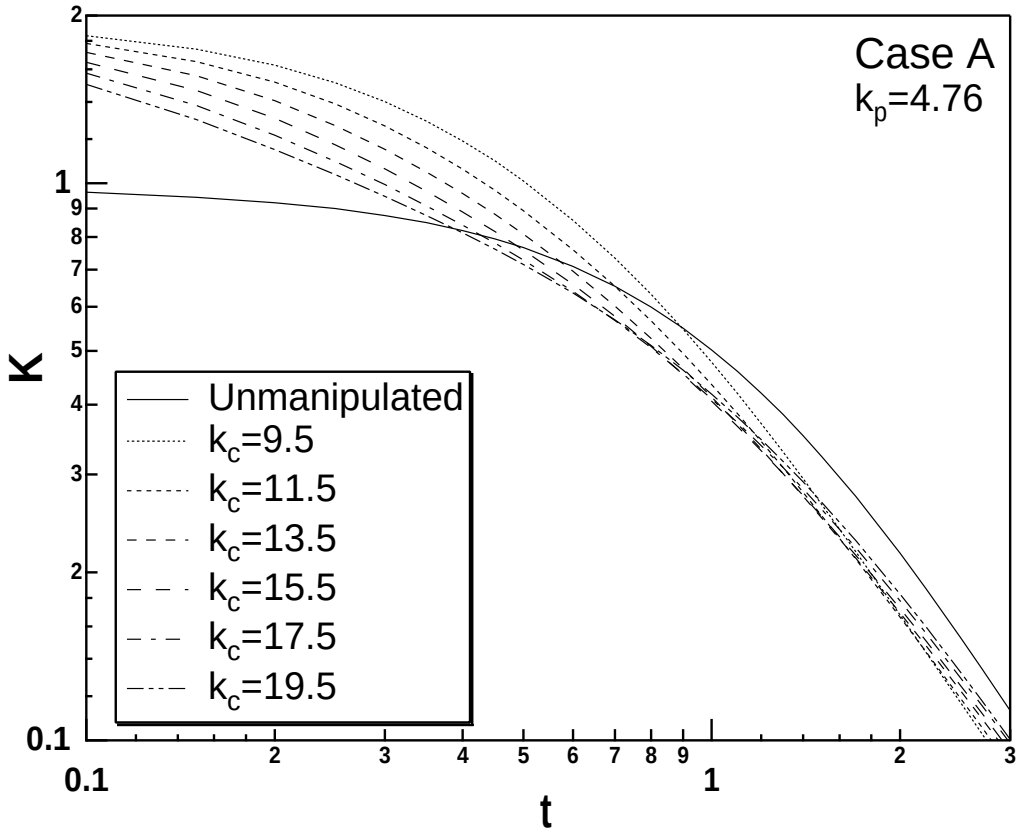

(b)

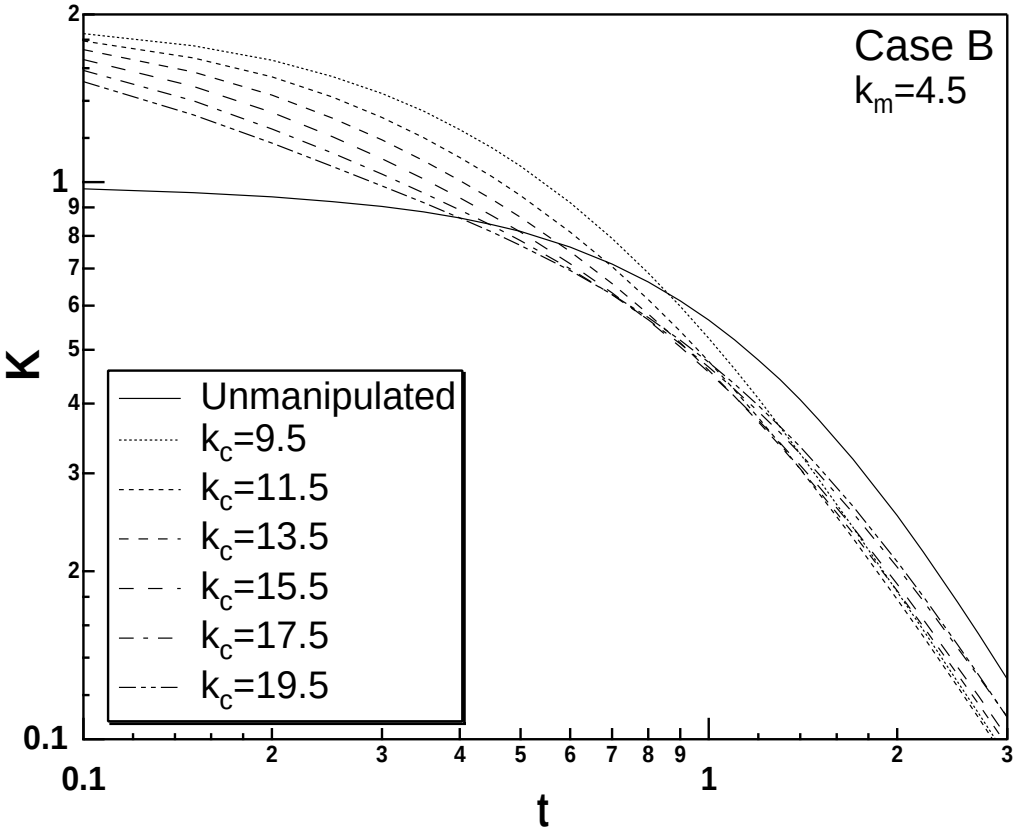

Figure 2: Time trace of turbulent kinetic energy. (a) Case A (k_p=4.76), (b) Case B (k_m=4.5).

(a)

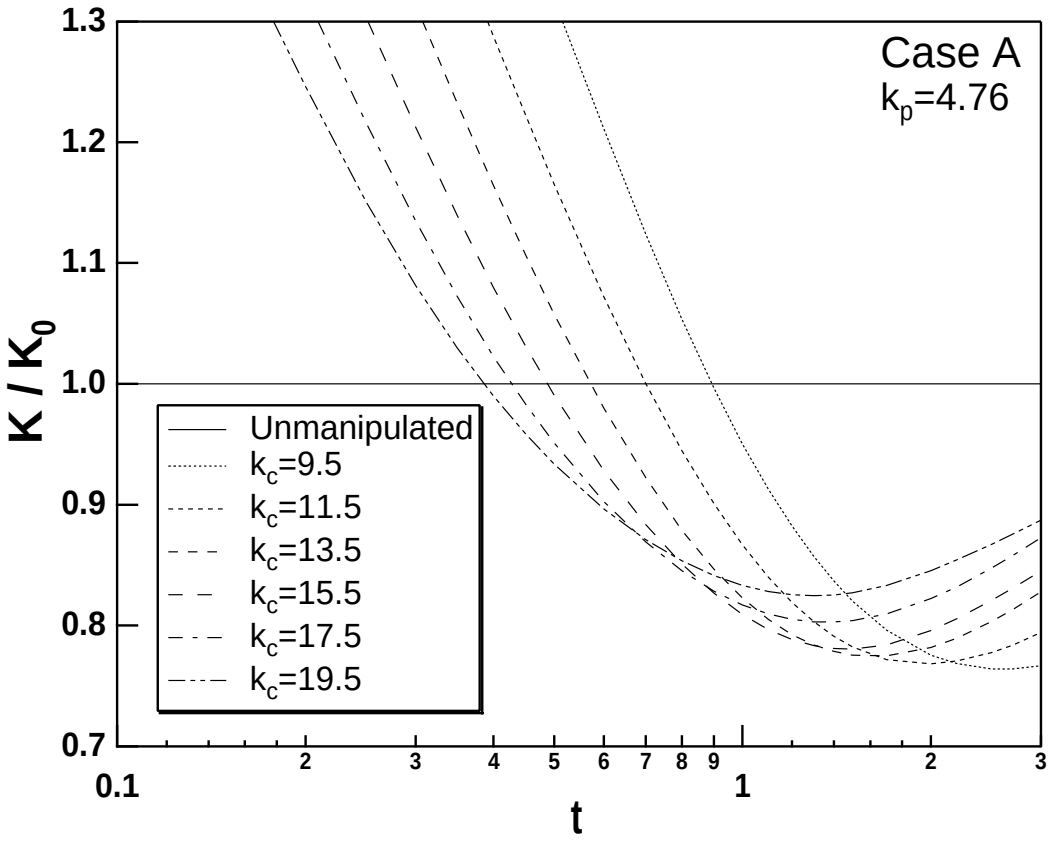

(b)

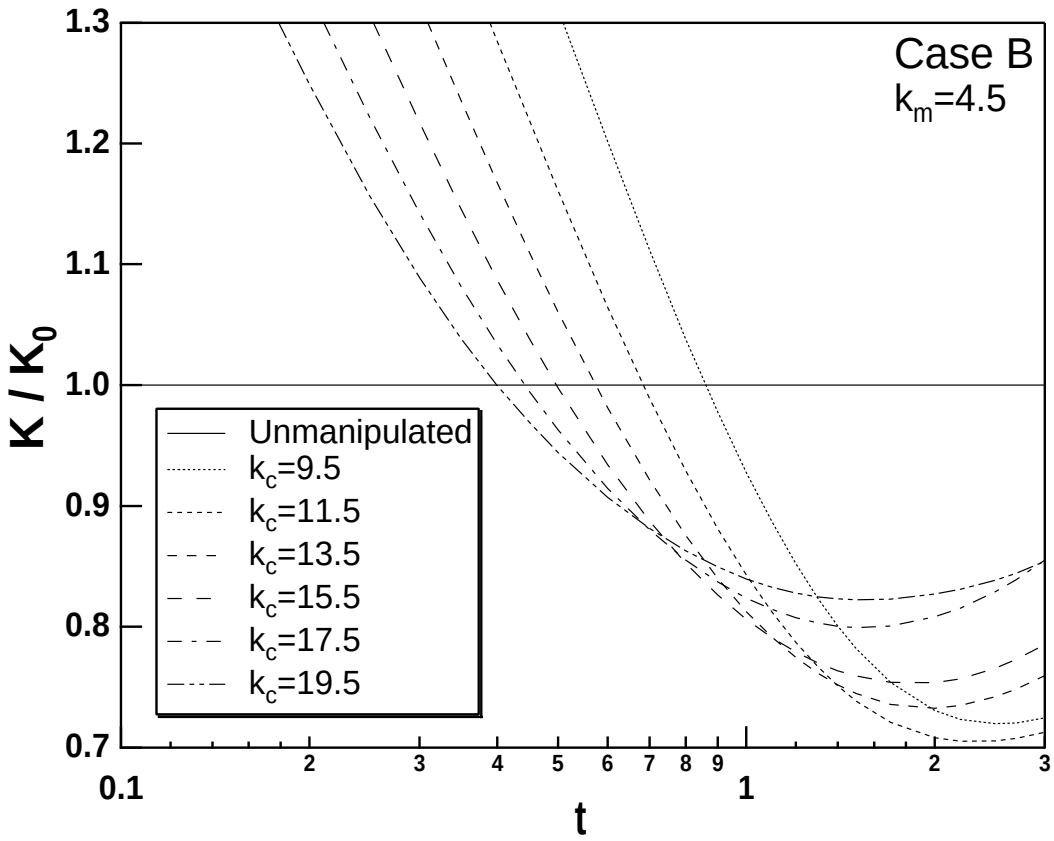

Figure 3: Time trace of turbulent kinetic energy normalized with that for the unmanipulated case. (a) Case A (k_p=4.76), (b) Case B (k_m=4.5).

(a)

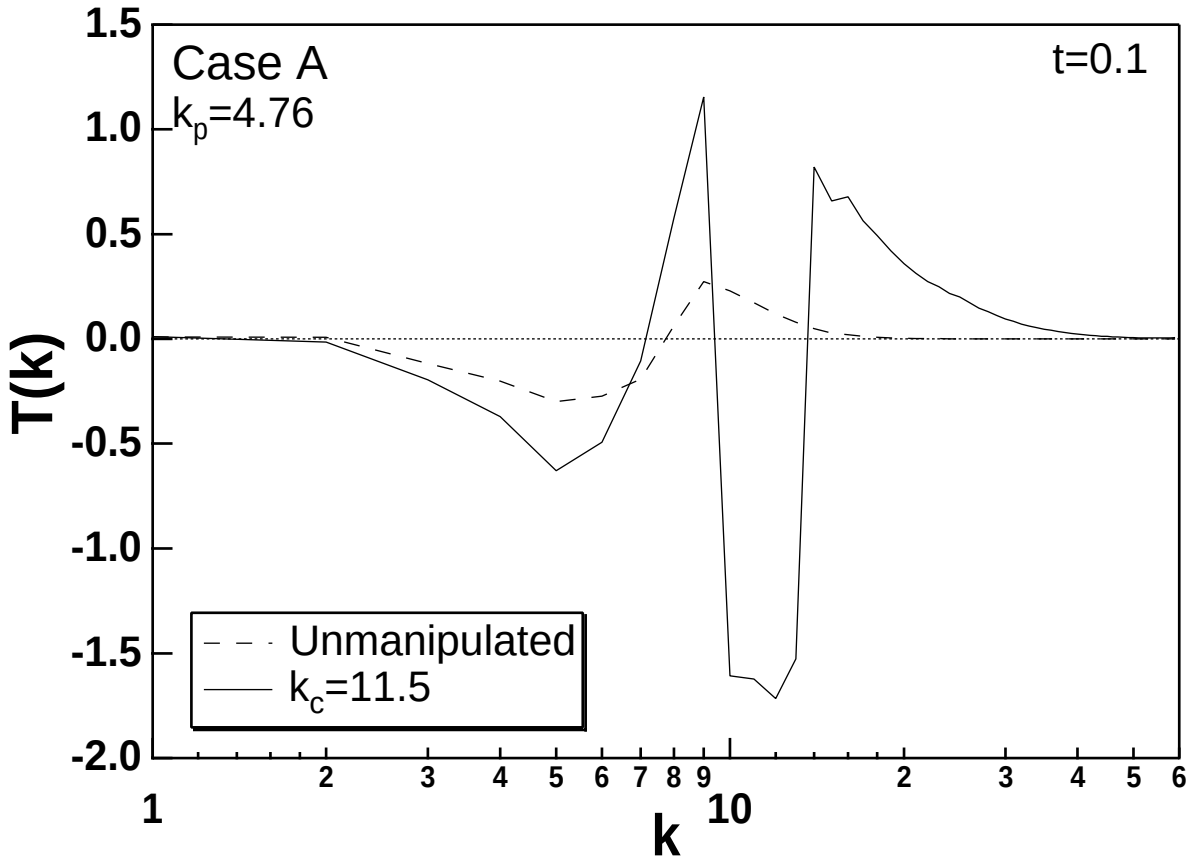

(b)

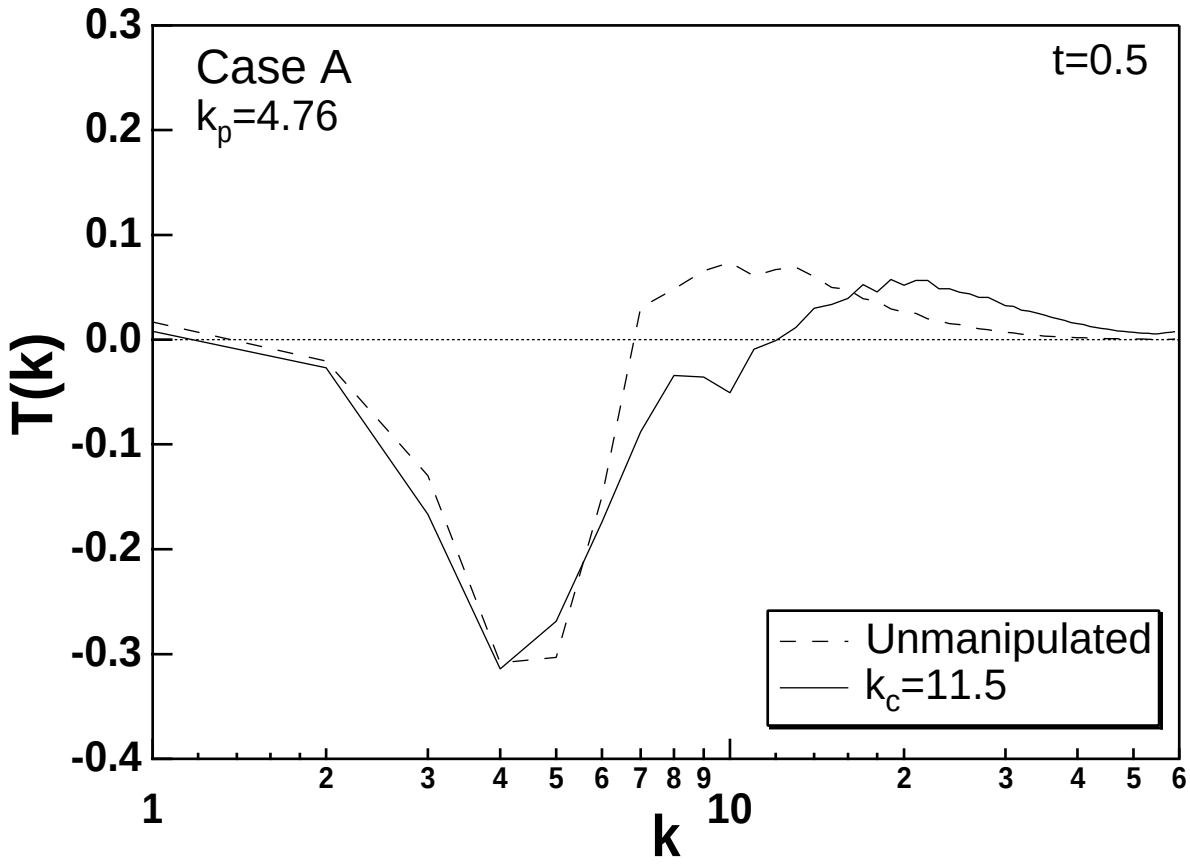

Figure 4: Temporal evolution of energy transfer function for Case A (k_p=4.76, k_c=11.5). (a)t=0.1, (b)t=0.5.

(c)

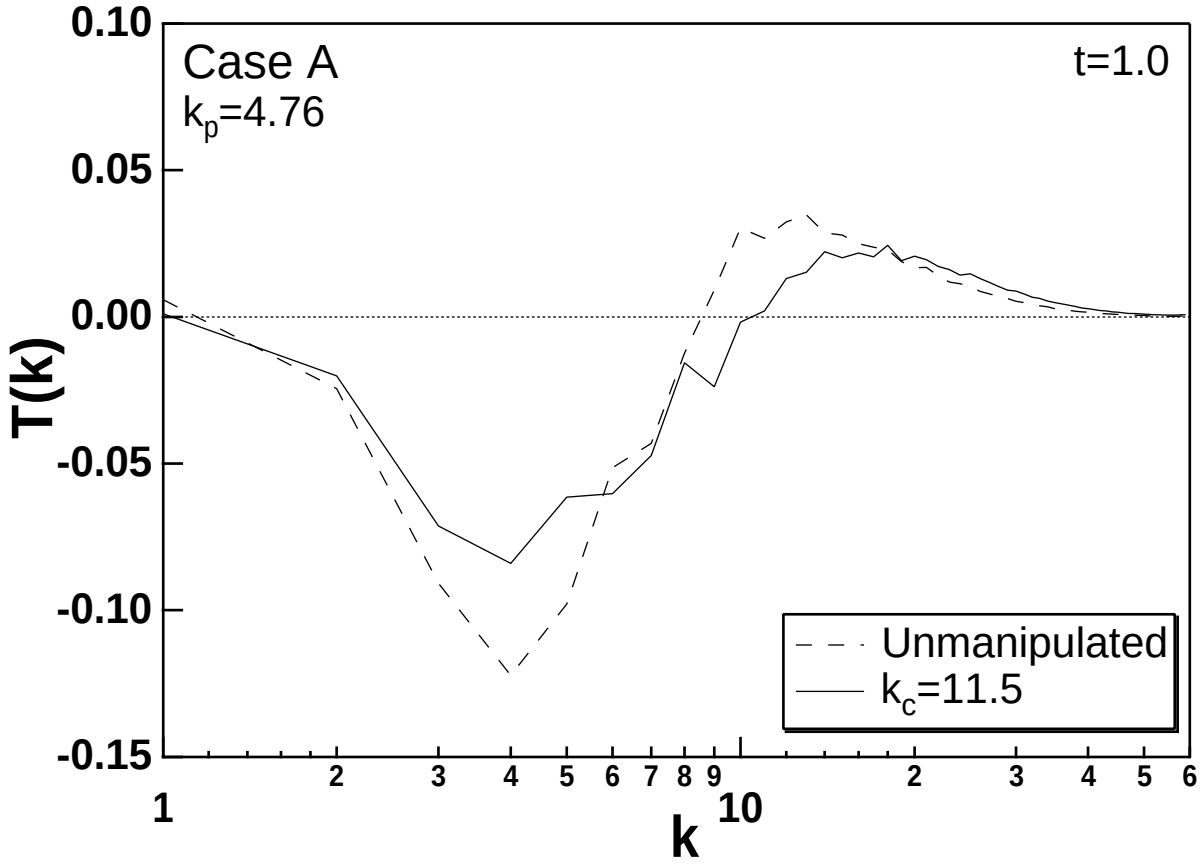

Figure 4: (c)*t*=1.0.

(a)

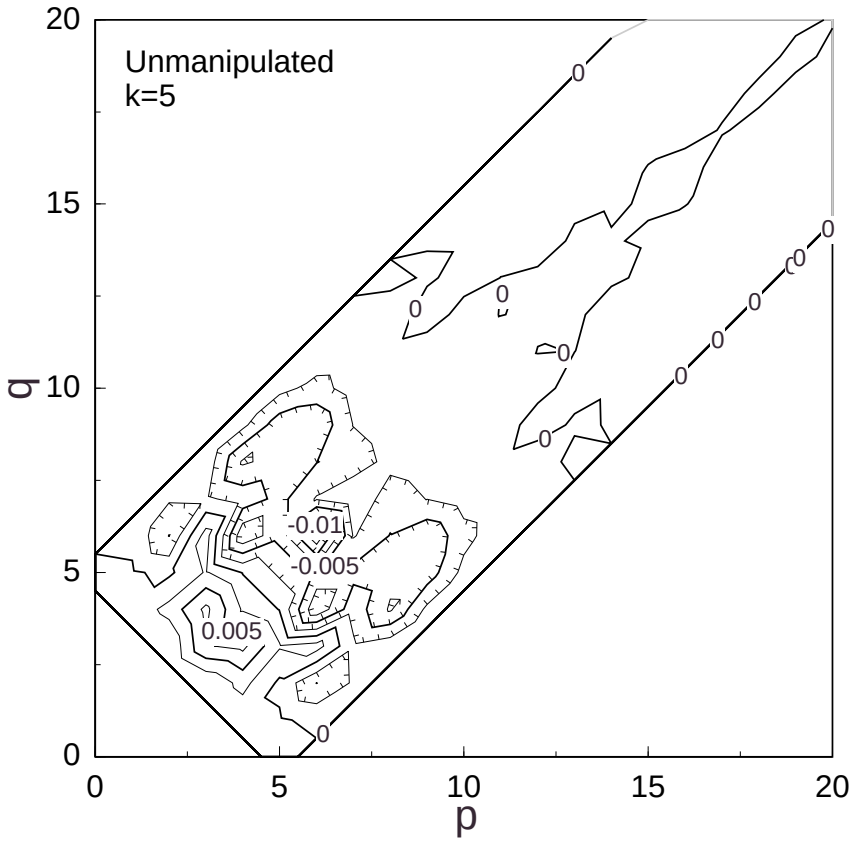

(b)

Figure 5: Triad transfer function for Case A (k_p=4.76, k=5) at t=0.1. (a)Unmanipulated case, (b) k_c=11.5.

(a)

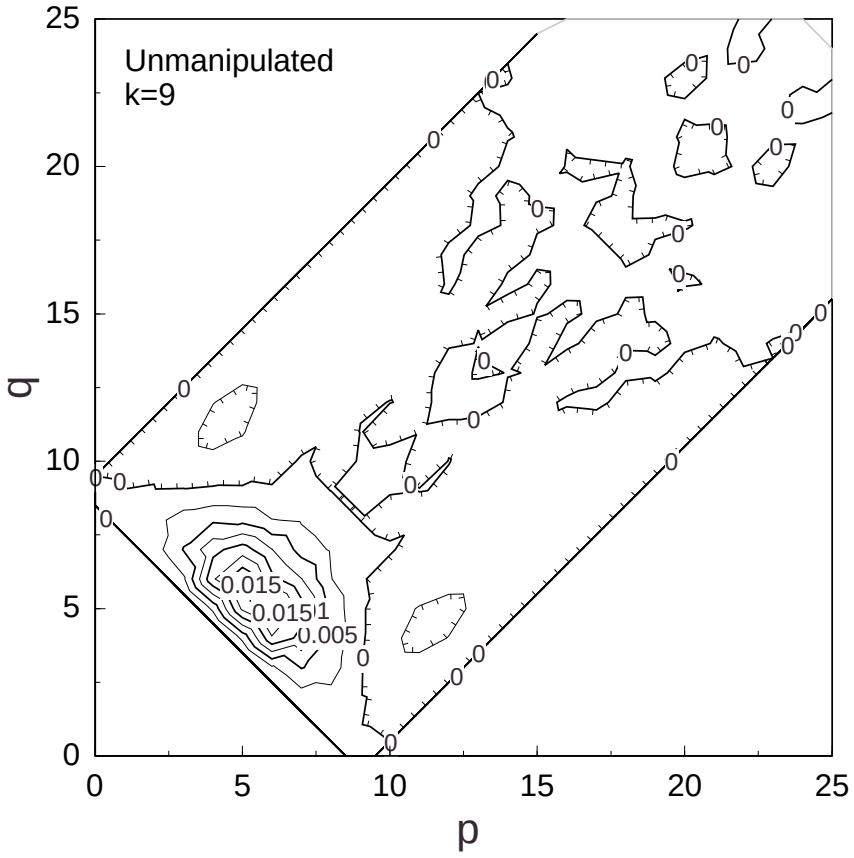

(b)

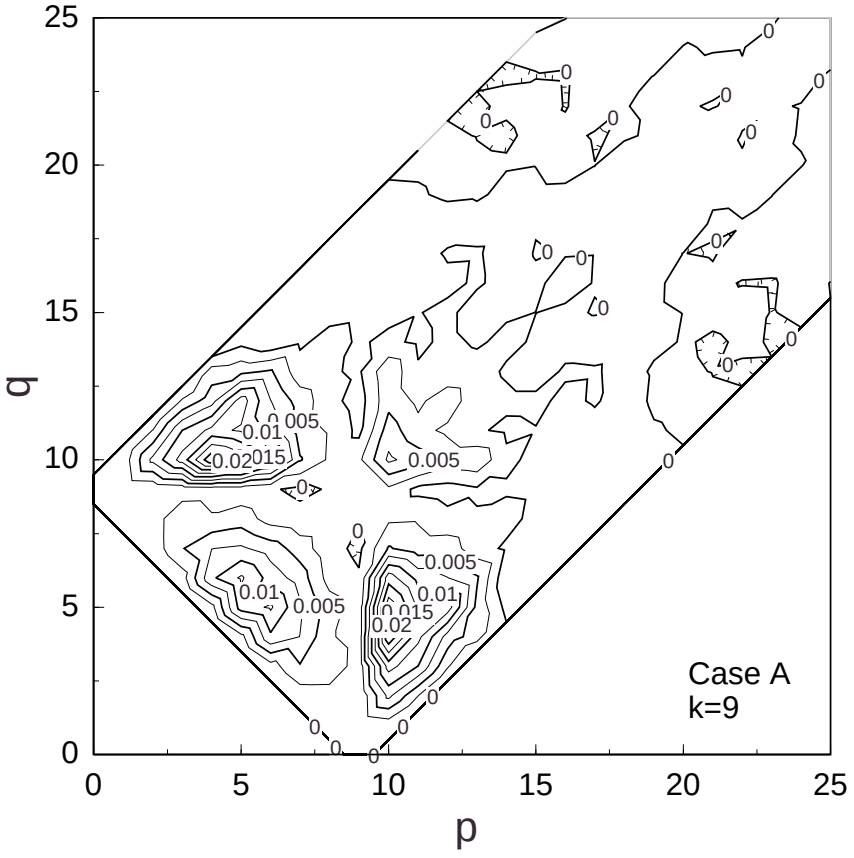

Figure 6: Triad transfer function for Case A (k_p=4.76, k=9) at t=0.1. (a)Unmanipulated case, (b) k_c=11.5.

(a)

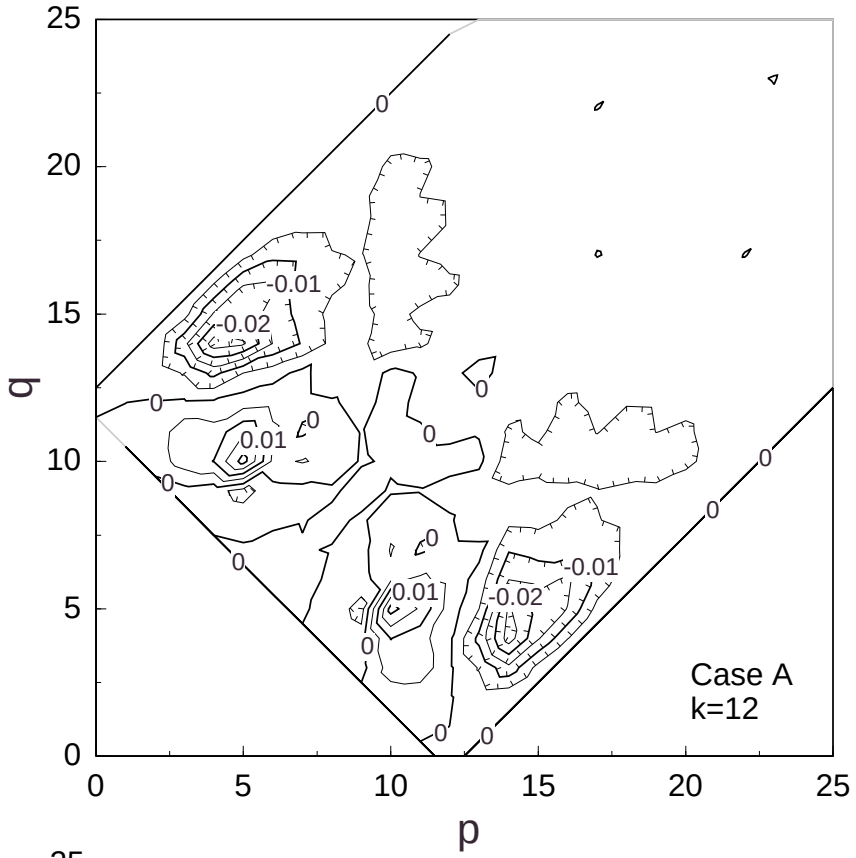

(b)

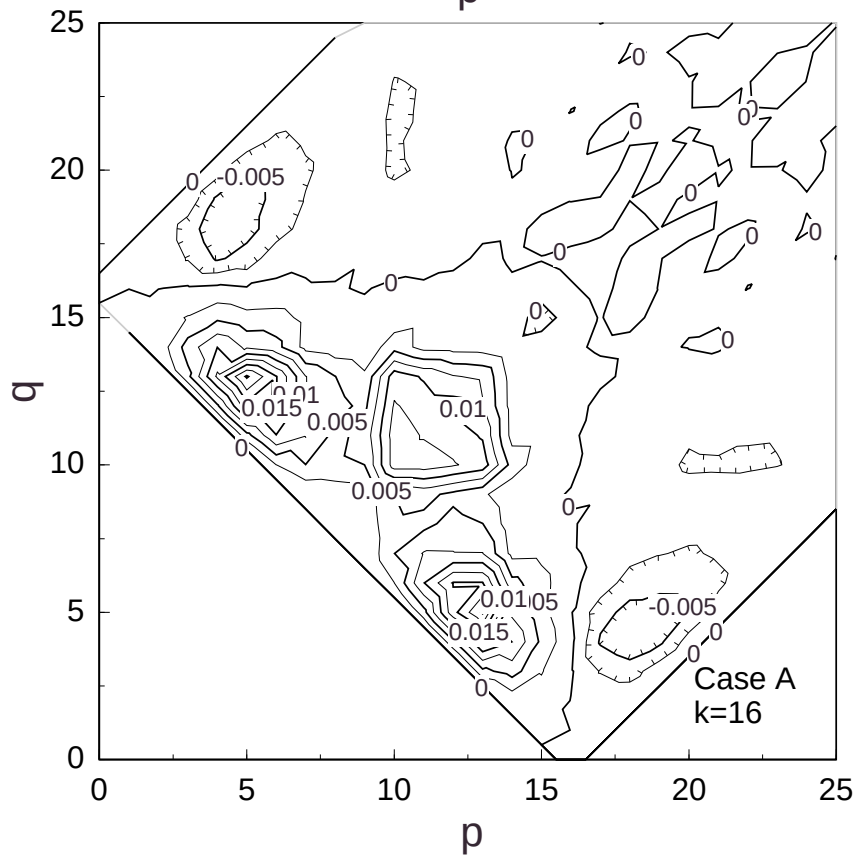

Figure 7: Triad transfer function for Case A (k_p=4.76, k_c=11.5) at t=0.1. (a)k=12, (b)k=16.

(a)

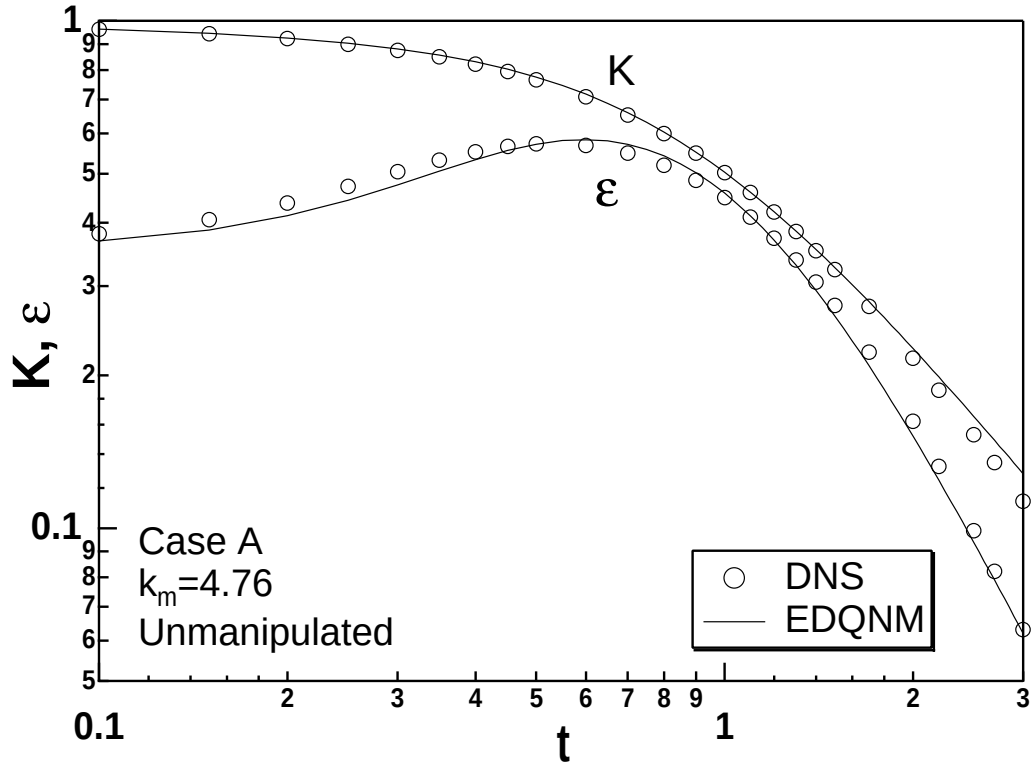

(b)

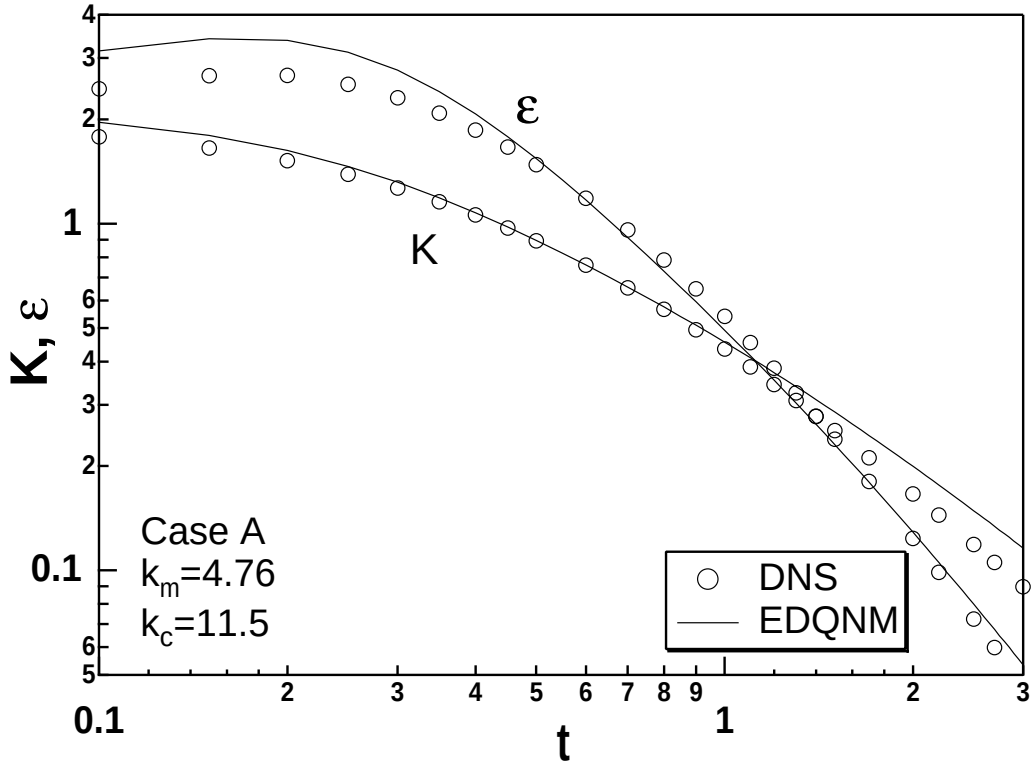

Figure 8: Time trace of turbulent kinetic energy and dissipation rate for Case A (k_p=4.76) for comparison of EDQNM and DNS. (a) Unmanipulated case, (b)k_c=11.5.

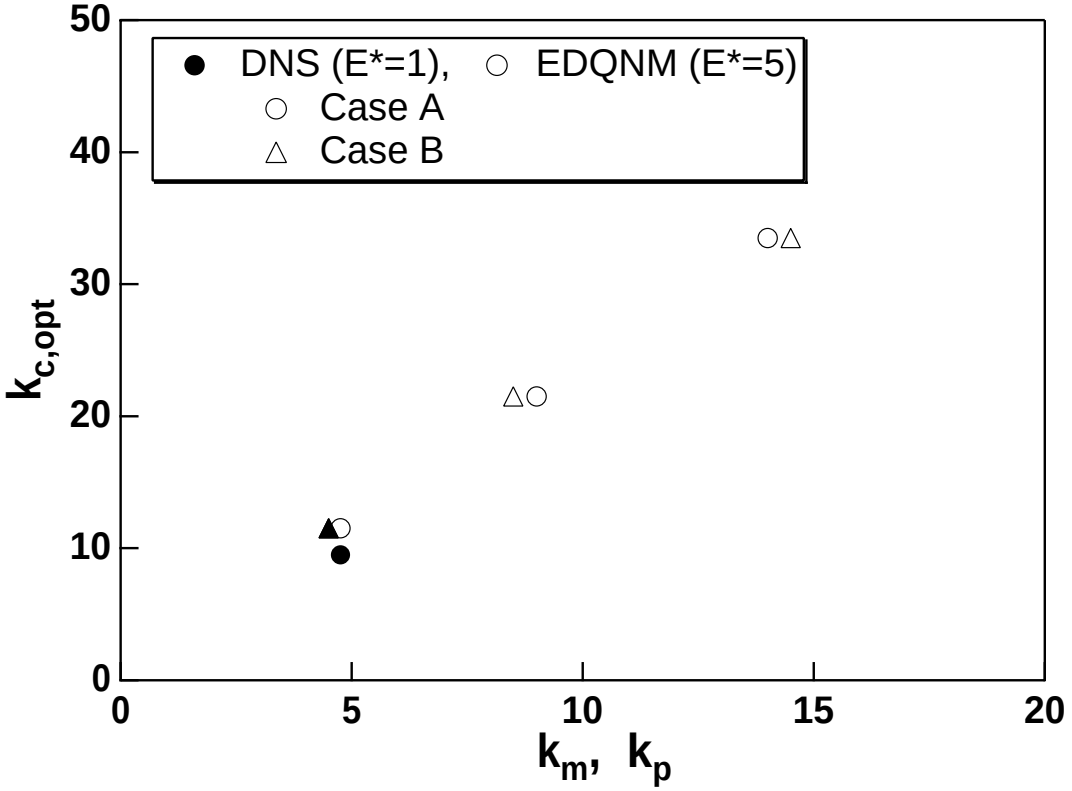

Figure 9: Optimum wave-number $k_{c,opt}$ versus characteristic wave-numbers for Cases A and B.

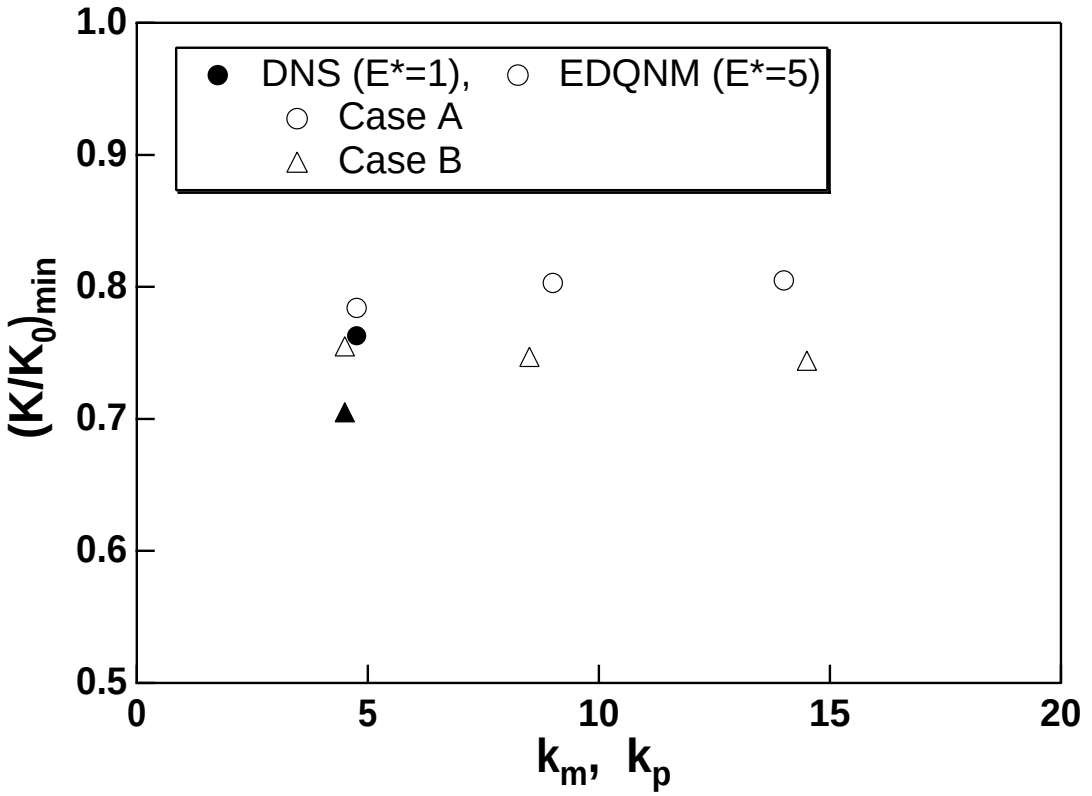

Figure 10: Mmaximum energy reduction rage $(K/K_0)_{\min}$ versus characteristic wave-numbers for Cases A and B.

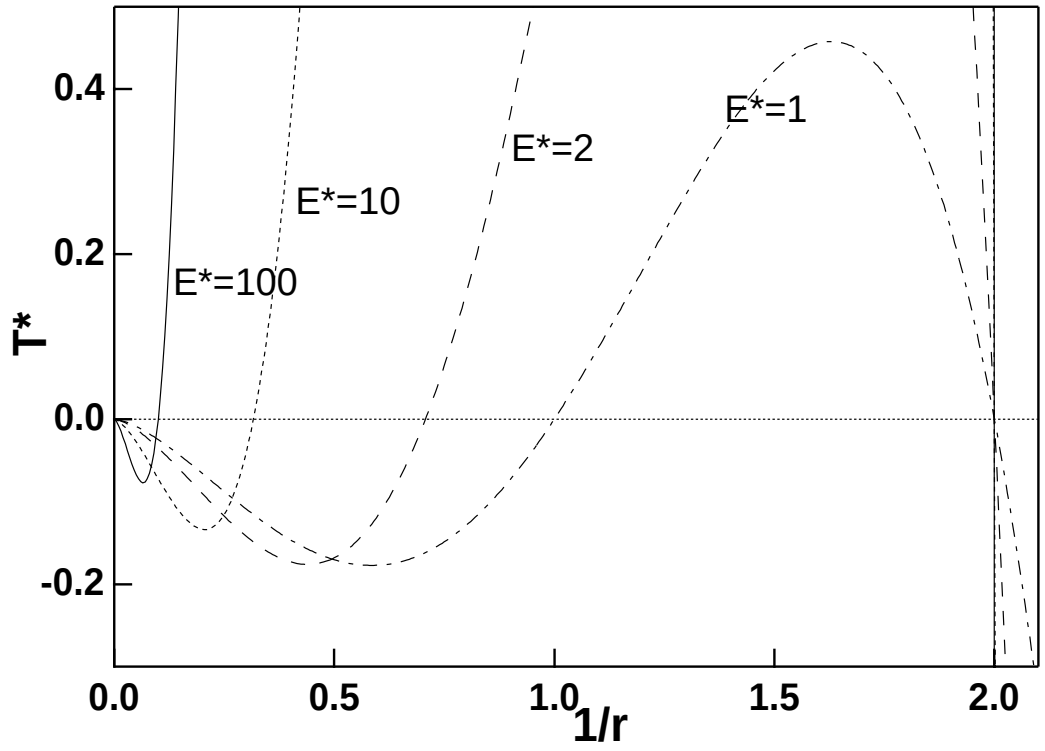

Figure 11: Distribution of nondimensionalized triad energy transfer function $T^*=T^*(r,E^*)$ of isosceles interactions.

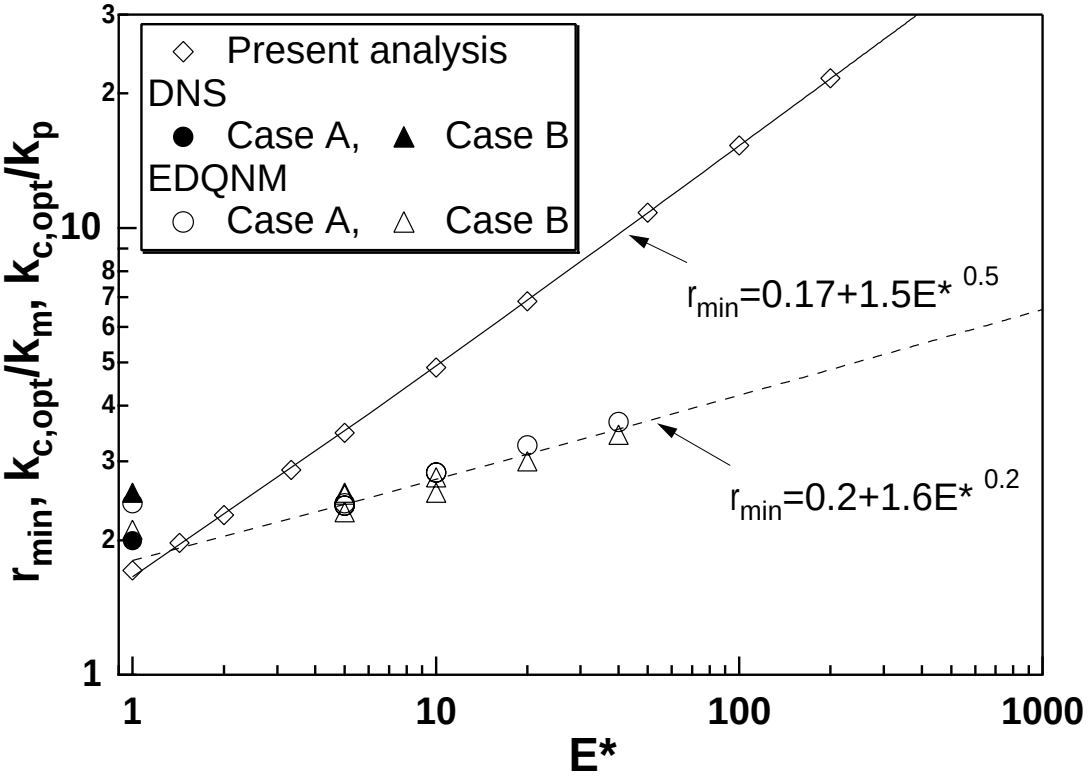

Figure 12: Optimum wave-number of control input versus turbulent energy ratio.

(a)

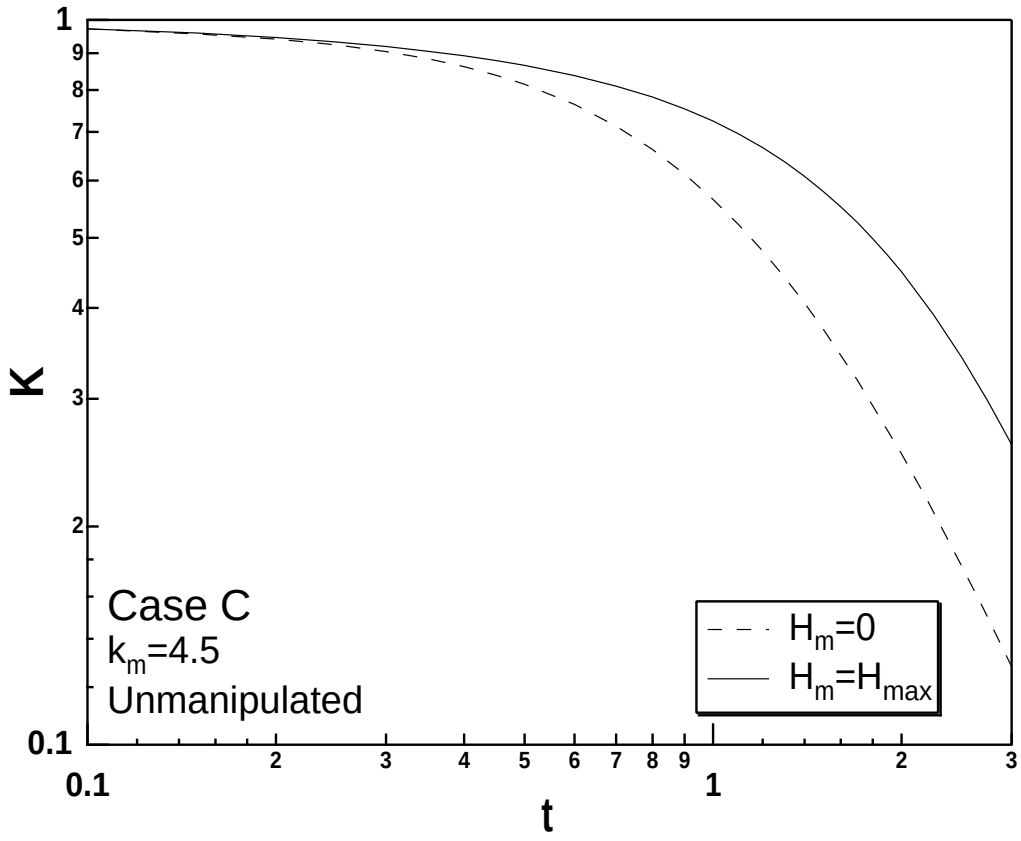

(b)

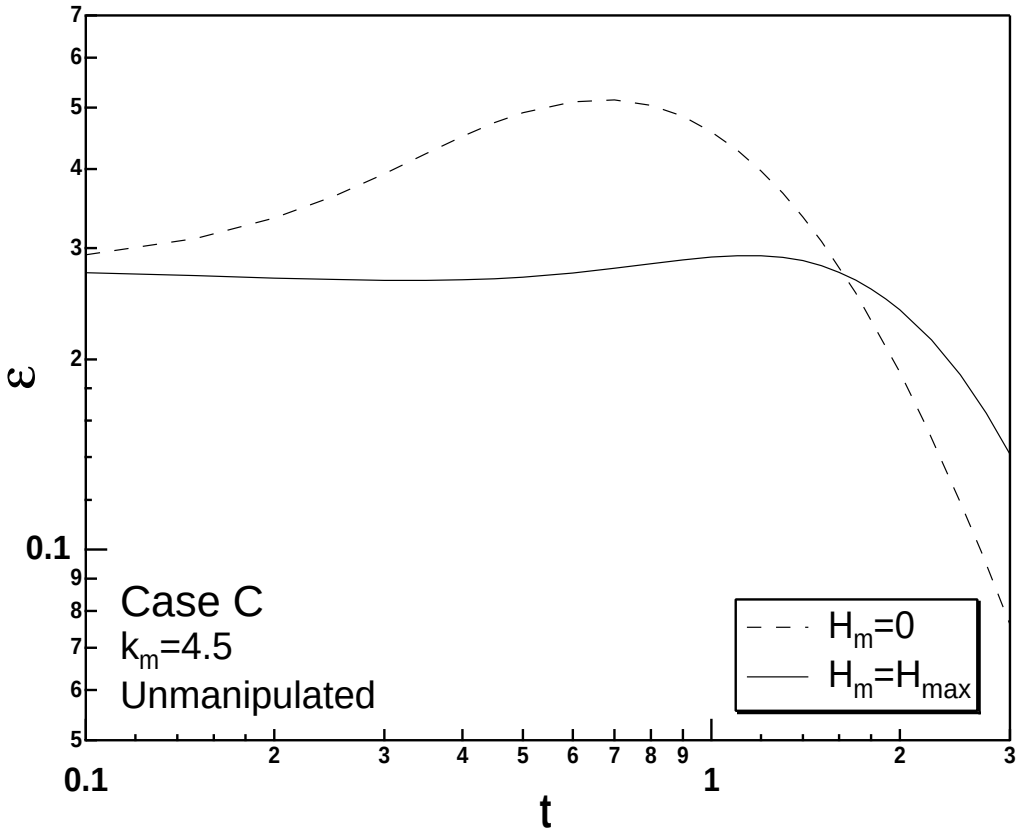

Figure 13: Time trace of turbulent energy *K* and its dissipation rate ε for Case C without control input. (a) *K* , (b) ε.

(a)

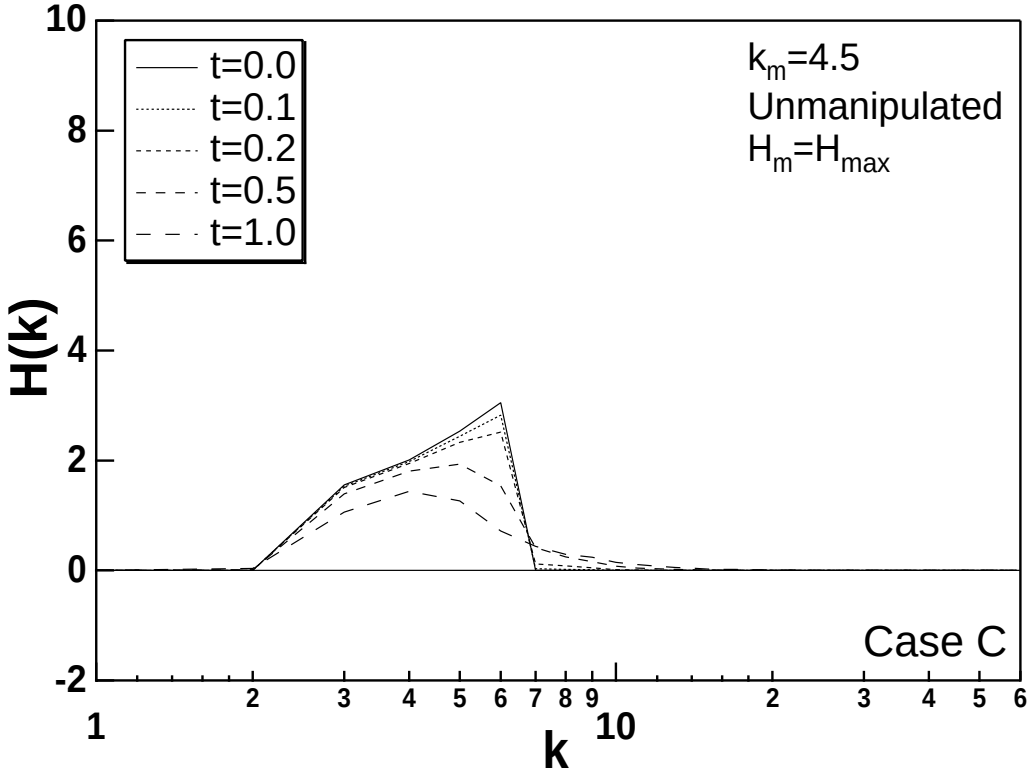

(b)

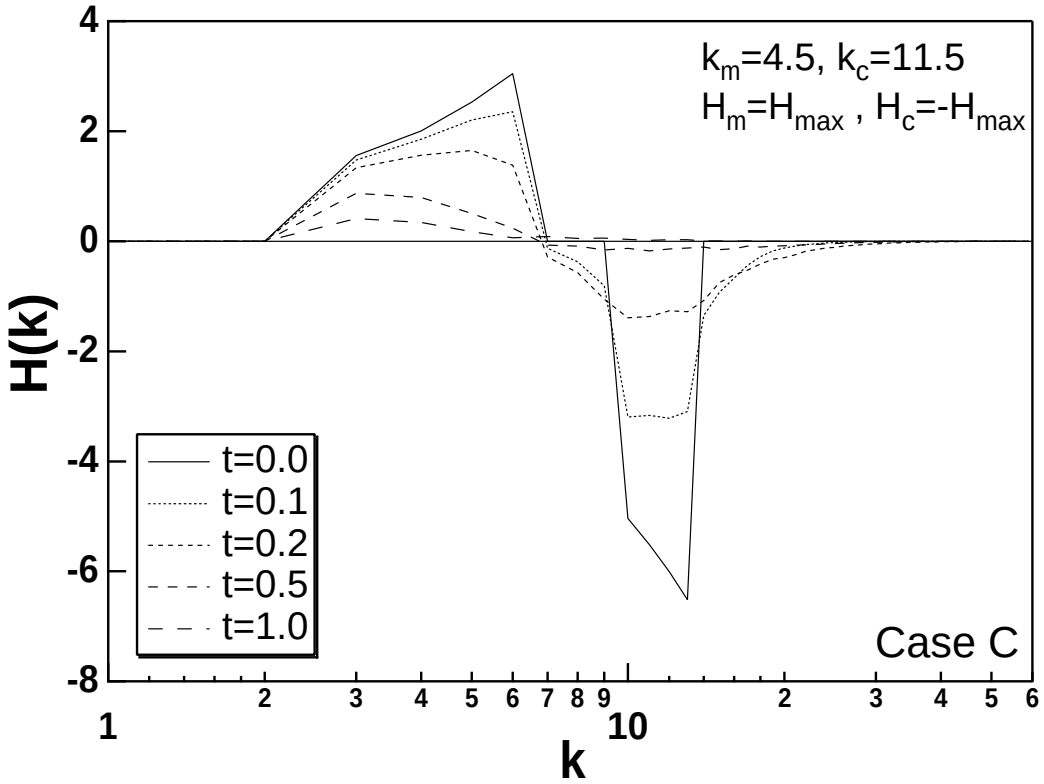

Figure 14: Temporal evolution of helicity spectral density for Case C. (a) Unmanipulated case, (b) H_c=-H_{max}.

(c)

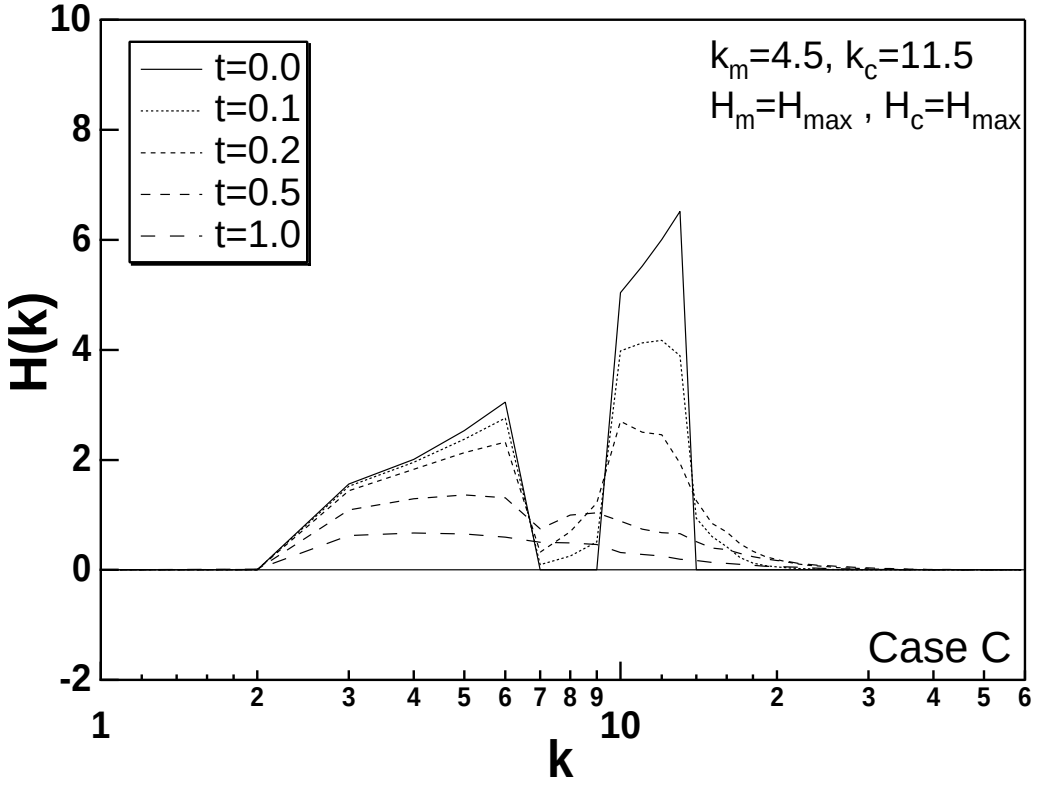

Figure 14: (c) H_c=H_{max}.

(a)

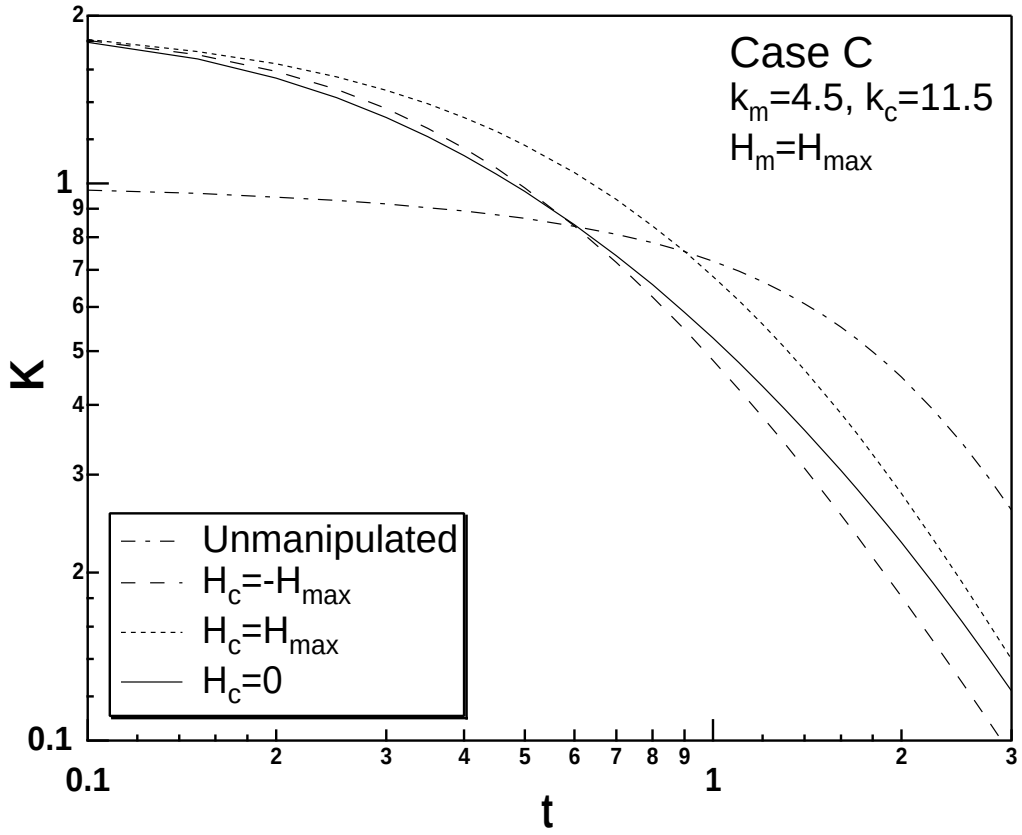

(b)

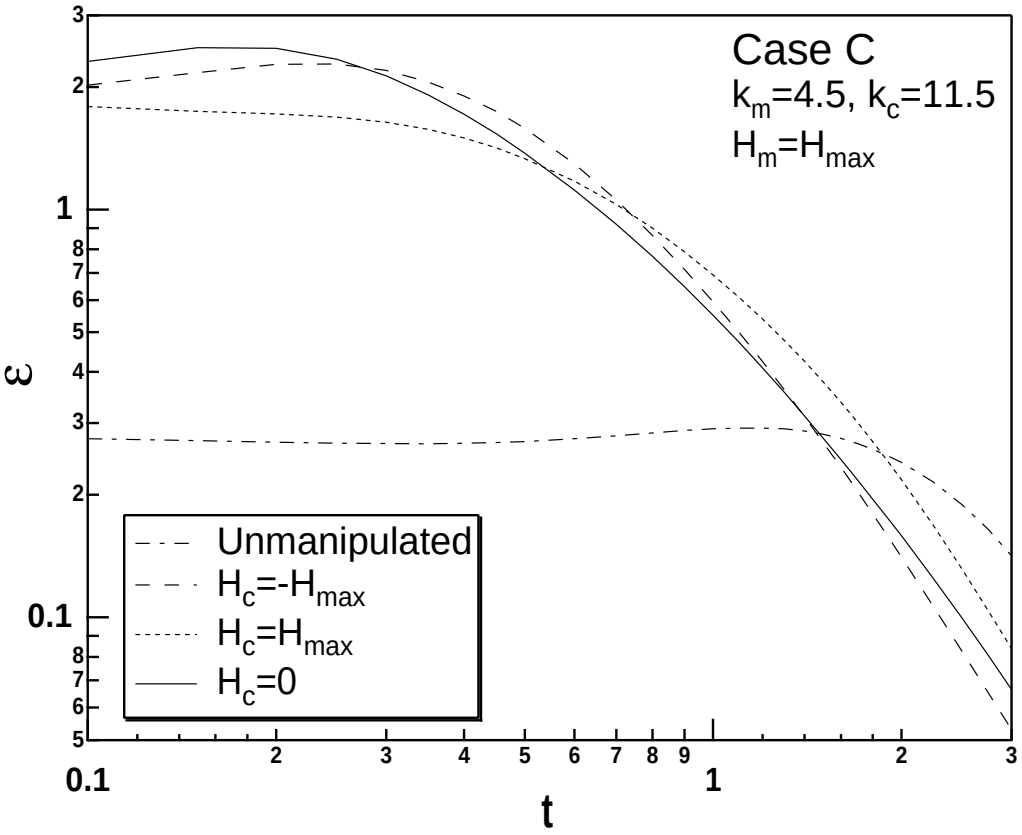

Figure 15: Time trace of turbulent kinetic energy *K* and its dissipation rate ε for Case C. (a) *K*, (b) ε.

(a)

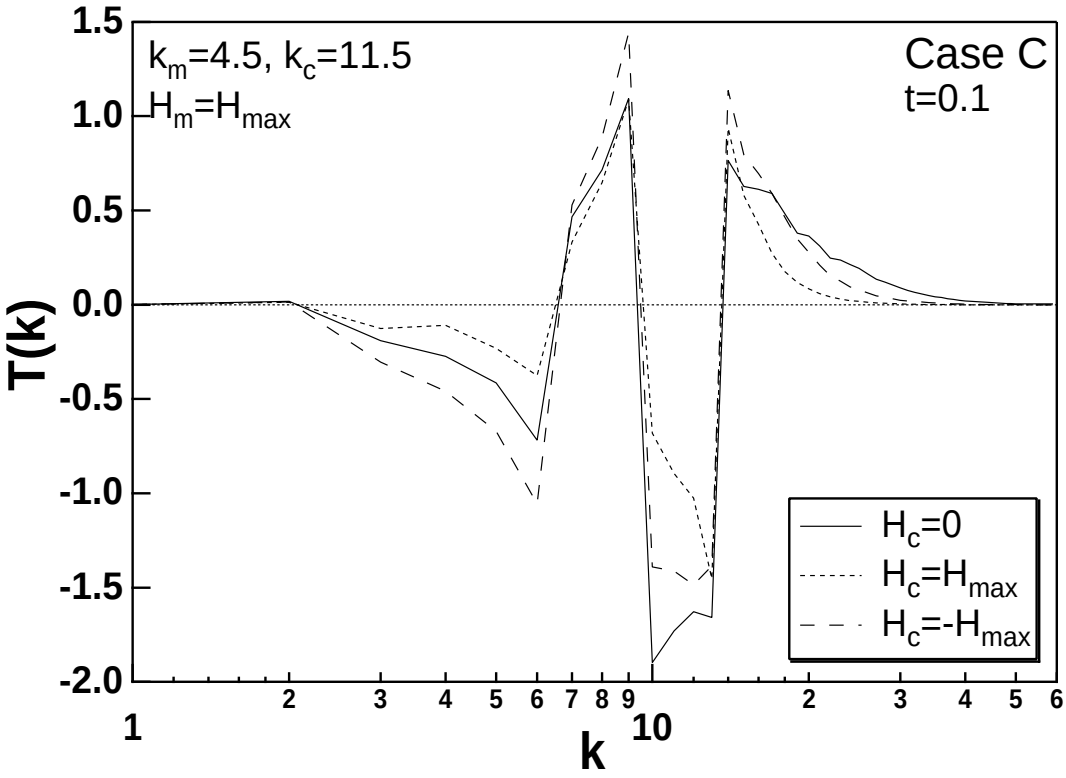

(b)

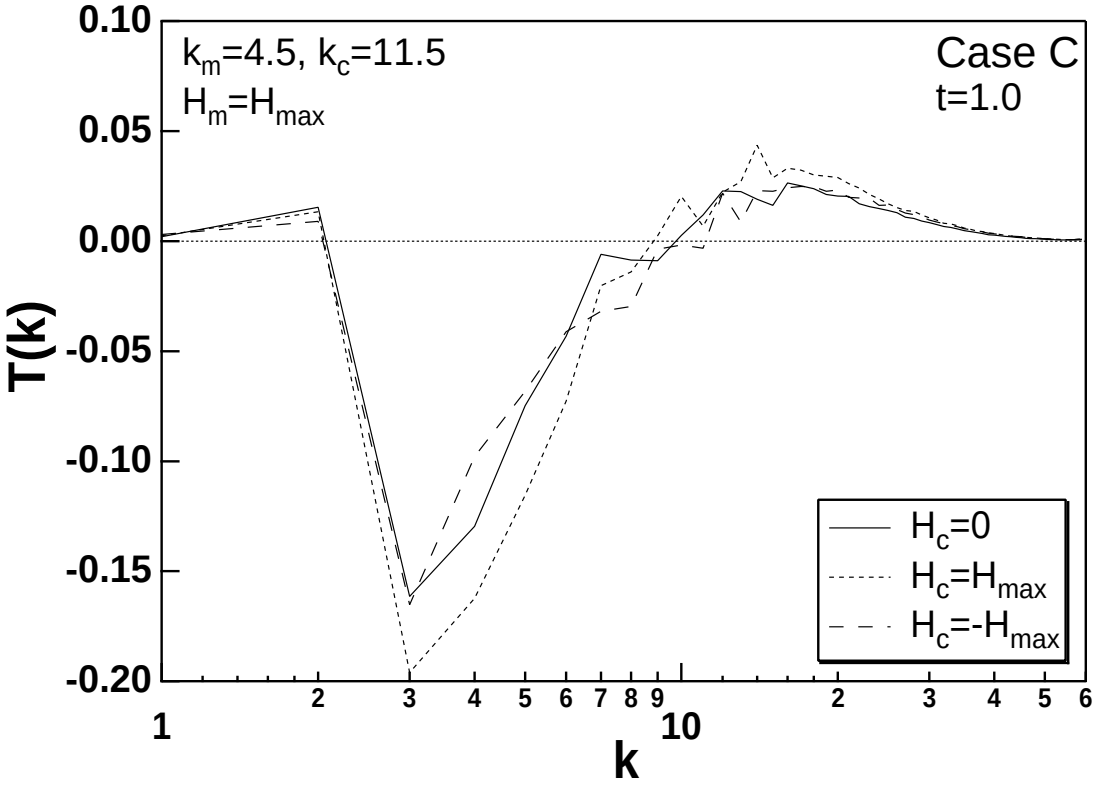

Figure 16: Temporal evolution of energy transfer function for Case C. (a)t=0.1, (b)t=1.0

(a)

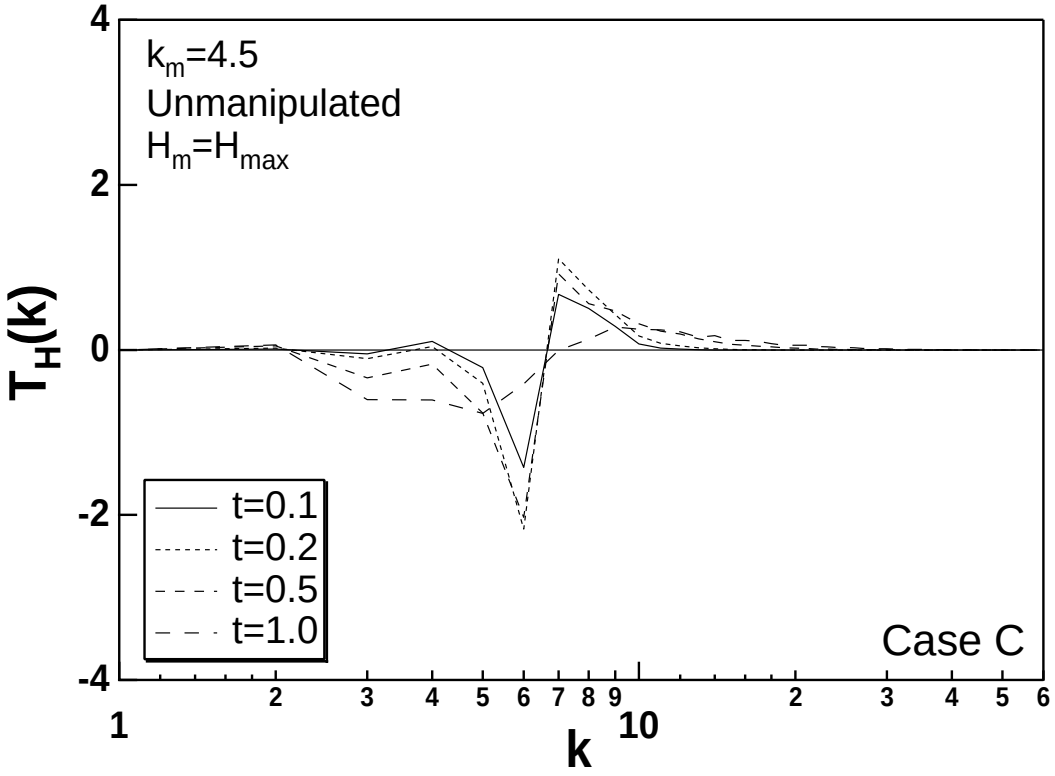

(b)

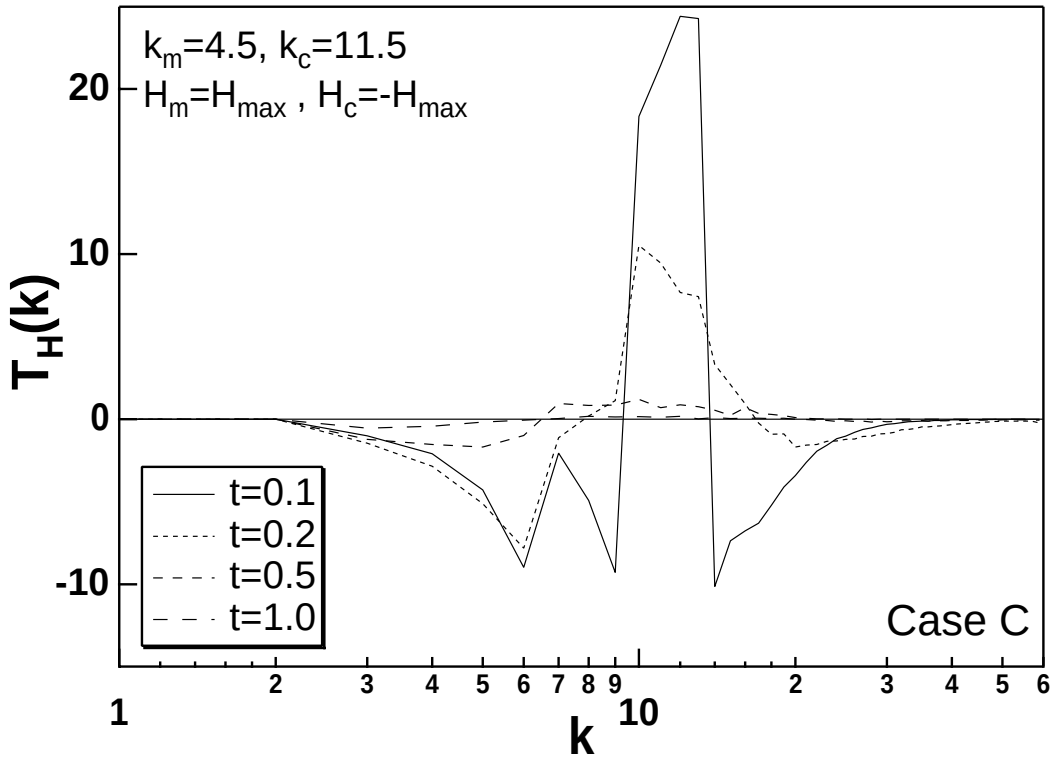

Figure 17: Temporal evolution of helicity transfer function for Case C. (a)$H_c=0$, (b)$H_c=-H_{max}$.

(c)

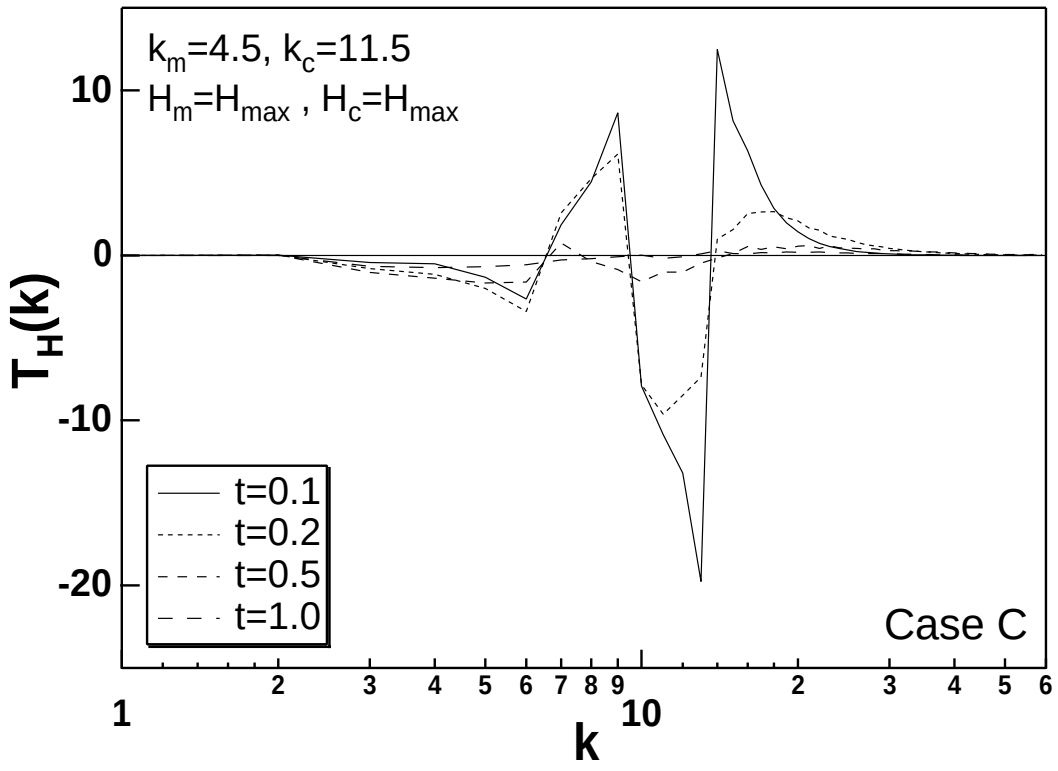

Figure 17: (c)H_c=H_{max}

(a)

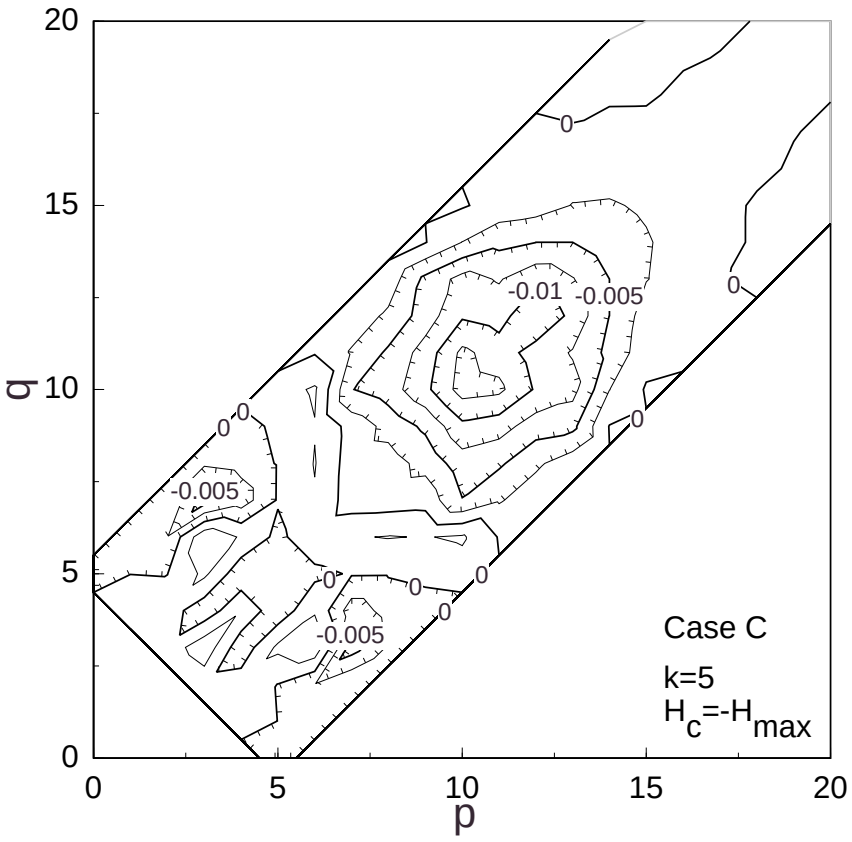

(b)

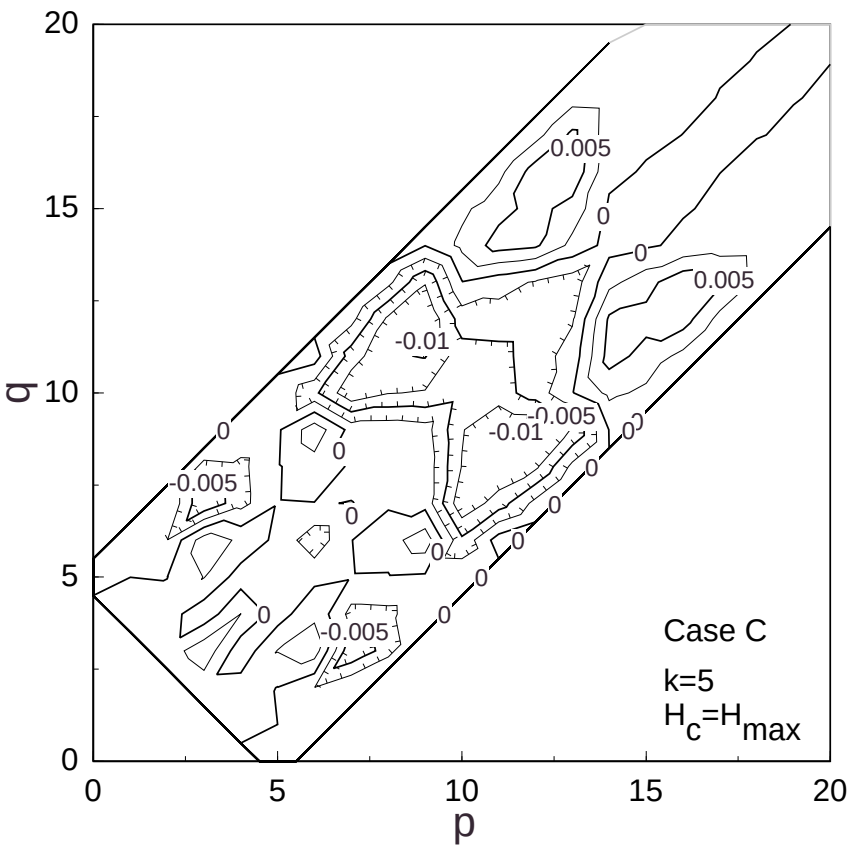

Figure 18: Triad transfer function for Case C at t=0.1. (a)H_c=-H_{max}, (b)H_c=H_{max}.

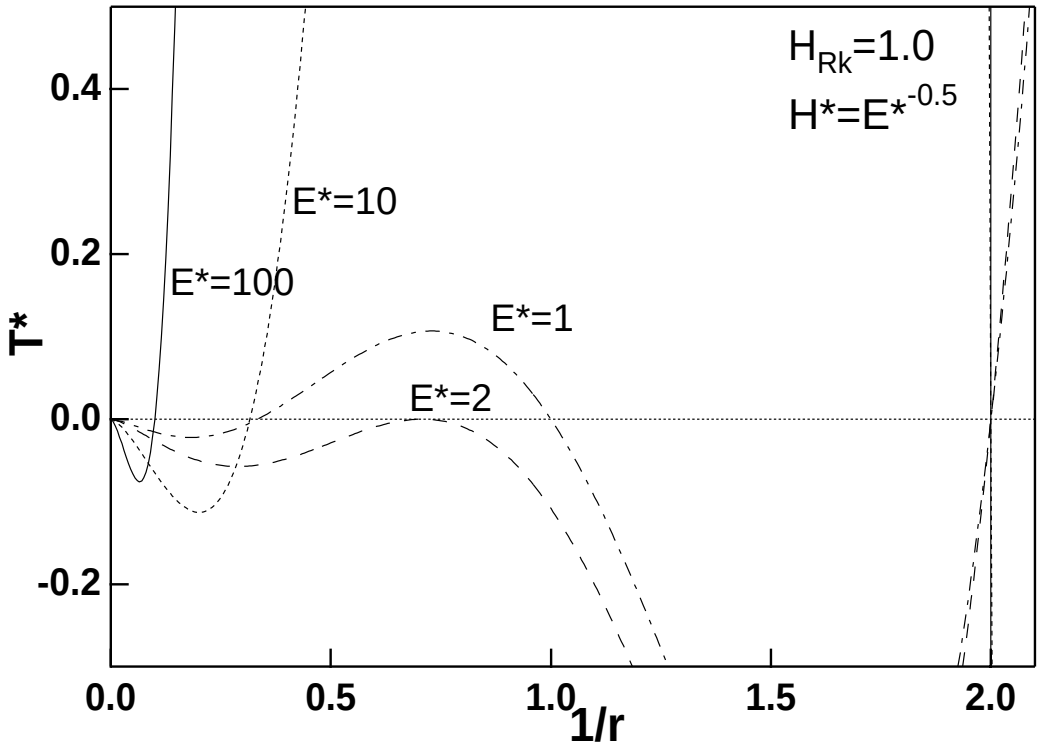

Figure 19: Distribution of nondimensionalized triad energy transfer function $T^*=T^*(r,E^*,H^*,H_{Rk})$ for helical case (H_{Rk}=1).